Water Resources Research

RESEARCH ARTICLE
10.1029/2020WR028134

Archetypes and Controls of Riverine Nutrient Export Across German Catchments

Pia Ebeling[1], Rohini Kumar[2], Michael Weber[2], Lukas Knoll[3], Jan H. Fleckenstein[1,4], and Andreas Musolff[1]

[1]Department of Hydrogeology, Helmholtz Centre for Environmental Research—UFZ, Leipzig, Germany, [2]Department of Computational Hydrosystems, Helmholtz Centre for Environmental Research—UFZ, Leipzig, Germany, [3]Institute for Landscape Ecology and Resources Management (ILR), Research Centre for BioSystems, Land Use and Nutrition (iFZ), Justus Liebig University Giessen, Giessen, Germany, [4]Bayreuth Center of Ecology and Environmental Research (BayCEER), University of Bayreuth, Bayreuth, Germany

Key Points:

- Riverine NO_3^- dynamics are controlled by vertical concentration heterogeneity, which can result from subsurface denitrification
- Diffuse P sources exert a strong control on the spatial variability of PO_4^{3-} export patterns in contrast to point sources
- Share of riparian wetlands controls the mean TOC concentrations in German catchments

Supporting Information:

Supporting Information may be found in the online version of this article.

Correspondence to:

P. Ebeling,
pia.ebeling@ufz.de

Citation:

Ebeling, P., Kumar, R., Weber, M., Knoll, L., Fleckenstein, J. H., & Musolff, A. (2021). Archetypes and controls of riverine nutrient export across German catchments. *Water Resources Research*, *57*, e2020WR028134. https://doi.org/10.1029/2020WR028134

Received 10 JUN 2020
Accepted 6 MAR 2021

Author Contributions:

Conceptualization: Pia Ebeling, Andreas Musolff
Data curation: Pia Ebeling, Rohini Kumar, Michael Weber, Lukas Knoll, Andreas Musolff
Formal analysis: Pia Ebeling, Rohini Kumar, Michael Weber, Andreas Musolff
Funding acquisition: Andreas Musolff
Investigation: Pia Ebeling
Methodology: Pia Ebeling, Rohini Kumar, Andreas Musolff
Supervision: Jan H. Fleckenstein, Andreas Musolff
Validation: Pia Ebeling
Visualization: Pia Ebeling

Abstract Elevated nutrient inputs challenge the health and functioning of aquatic ecosystems. To improve riverine water quality management, it is necessary to understand the underlying biogeochemical and physical processes, anthropogenic drivers and their interactions at catchment scale. We hypothesize that the spatial heterogeneity of nutrient sources dominantly controls the variability of in-stream concentration dynamics among catchments. We investigated controls of mean nitrate (NO_3^-), phosphate (PO_4^{3-}), and total organic carbon (TOC) concentrations and concentration-discharge (*C*-*Q*) relationships in 787 German catchments of a newly assembled data base, covering a wide range of physiographic and anthropogenic settings. We linked water quality metrics to catchment characteristics using partial least squares regressions and random forests. We found archetypal *C*-*Q* patterns with enrichment dominating NO_3^- and TOC, and dilution dominating PO_4^{3-} export. Both the mean NO_3^- concentrations and their variance among sites increased with agricultural land use. We argue that subsurface denitrification can buffer high nitrogen inputs and cause a decline in concentration with depth, resulting in chemodynamic, strongly positive *C*-*Q* patterns. Mean PO_4^{3-} concentrations were related to point sources, though the low predictive power suggests effects of unaccounted in-stream processes. In contrast, high diffuse agricultural inputs explained observed positive PO_4^{3-} *C*-*Q* patterns. TOC levels were positively linked to the abundance of riparian wetlands, while hydrological descriptors were important for explaining TOC dynamics. Our study shows a strong modulation of anthropogenic inputs by natural controls for NO_3^- and PO_4^{3-} concentrations and dynamics, while for TOC only natural controls dominate observed patterns across Germany.

Plain Language Summary Phosphorus, nitrogen, and organic carbon are key elements of plants and all living organisms. Humans are altering the nutrient cycles especially, to improve agricultural productivity and through domestic and industrial wastewater. Excess nutrients in surface waters have harmed many aquatic ecosystems by causing toxic algal blooms and a loss of biodiversity. Low nutrient concentrations and habitat variability are similarly important to those ecosystems, but human interference with natural drivers is not yet fully understood. To better understand and disentangle natural or human controls, we investigated nutrient concentrations and their variability across German catchments with varying landscapes and anthropogenic conditions. The human impact is clearly visible for mean nitrate concentrations, while the (natural) subsurface properties mainly controlled the variability of riverine nitrate. In the past, phosphate inputs were usually linked to wastewater, yet we found the control of agricultural activities on concentration dynamics to be unexpectedly high. Organic carbon was mainly associated with natural sources related to riparian wetlands where interactions with other nutrients are possible. This understanding of dominant controls is important in order to adapt management strategies to ensure healthy aquatic ecosystems.

1. Introduction

Elevated nutrient inputs from human sources such as fertilizers and wastewater put aquatic ecosystems under pressure. The health and functioning of stream ecosystems and the eutrophication risk are strongly linked to nutrient concentrations (Conley et al., 2009; Galloway et al., 2003; Vitousek et al., 1997), while

Writing – original draft: Pia Ebeling
Writing – review & editing: Pia Ebeling, Rohini Kumar, Michael Weber, Lukas Knoll, Jan H. Fleckenstein, Andreas Musolff

their temporal variability can additionally affect the pressure and reversibility of effects (Withers & Jarvie, 2008) and primary production via for example stoichiometric shifts (Conley et al., 2009). Moreover, the dynamics of nutrient concentrations in concert with discharge variability control nutrient loads exported from catchments to downstream water bodies and cause eutrophication in many receiving rivers, lakes, and estuaries around the globe (e.g., Bricker et al., 1999; EEA, 2018; Jenny et al., 2020).

Several national and European regulations have been adopted to reduce water quality problems with a major focus on the macronutrients nitrogen (N) and phosphorous (P). Initially, the regulations in Europe and the USA focused on reducing nutrient inputs related to point sources (BGBI.1, 1980; Copeland, 2016; EEC, 1991a), but later additionally addressed nonpoint-source pollution (Copeland, 2016; EEC, 1991b, 2000). In Europe, the Water Framework Directive (WFD, EEC, 2000) set water quality aims and guidelines including the reduction of diffuse N and P pollution and the demand for a river basin and ecology-oriented perspective for water quality management. Still, many surface water bodies worldwide lack a good ecological status, with diffuse agricultural sources being one of the main pressures (Damania et al., 2019; EEA, 2018; EPA, 2017). Even though regulations do not focus on regulating the macronutrient organic carbon (Stanley et al., 2012), it affects aquatic ecosystem structure and functioning (for example via energy input and biogeochemical interactions) and can impair drinking water resources (Solomon et al., 2015).

Measures to improve water quality are usually implemented and evaluated at catchment scale (Bouraoui & Grizzetti, 2011). Catchments are complex systems with various biogeochemical and hydrological processes interacting at different spatial and temporal scales (Bouwman et al., 2013; Clark et al., 2010) and finally integrating into water quantity and quality responses at the catchment outlet (Bouraoui & Grizzetti, 2011). A considerable amount of nutrients can be retained or transformed in different compartments, such as soils, groundwater, riparian zones, and streams, altogether considered as successive filters which alter specific loads transported downstream (Bouwman et al., 2013). The importance of processes on transported loads generally depends on the interplay between transport and reaction time scales (Musolff et al., 2017; Oldham et al., 2013). Hierarchies and interactions among processes and different scales as well as differences among catchments are still not properly understood, and upscaling of small-scale processes to the catchment scale remains a challenging task (Bol et al., 2018; Pinay et al., 2015). The integrated signal of concentration (C), discharge (Q) and their relationship observed at the catchment outlet can be used to characterize catchment functioning, to reveal generalities and differences among solutes and catchments and thereby to interpret underlying processes (Sivapalan, 2006).

Mean concentrations indicate the general levels of nutrient stress, while concentration-discharge (C-Q) relationships classify solute export dynamics in terms of export regimes and patterns (Musolff et al., 2015). A chemostatic regime can be defined as low C variability compared to high Q variability, while a chemodynamic regime refers to a high C to Q variability using e.g. the coefficients of variation (CV) (Thompson et al., 2011). Export patterns characterize the direction and strength of influence of Q on C. Enrichment patterns describe increasing C with increasing Q, while dilution describes decreasing C with increasing Q, which prevail in supply limited systems. When comparing C-Q relationships among different solutes and catchments, generalities and key controls of solute export can be identified (Minaudo et al., 2019; Musolff et al., 2015; Zarnetske et al., 2018). C-Q relationships have been widely applied at different temporal scales, that is at event, inter- and intra-annual scales (Dupas et al., 2016; Minaudo et al., 2019; Rose et al., 2018; Westphal et al., 2019), and spatial scales, i.e. from hillslopes and headwaters (e.g. Bishop et al., 2004; Herndon et al., 2015; Hunsaker & Johnson, 2017) to numerous, large and nested catchments (e.g. Basu et al., 2010; Evans et al., 2014; Moatar et al., 2020).

To understand riverine nutrient export dynamics, we require process understanding of the major components of catchment scale transport—input, mobilization and retention. Mean nitrate (NO_3) concentrations in general increase with higher shares of agricultural land (e.g., Evans et al., 2014; Hansen et al., 2018; Minaudo et al., 2019; Musolff et al., 2015). However, elevated N inputs can be counteracted by removal, for example via denitrification under anoxic conditions and sufficient availability of electron donors, as observed in wetlands (Hansen et al., 2018), riparian zones (Pinay et al., 2015; Sabater et al., 2003) and groundwater (Rivett et al., 2008). Elevated phosphate (PO_4^{3-}) concentrations have been mainly related to point sources (Minaudo et al., 2019; Westphal et al., 2019), though with significant point source reductions diffuse P emissions from agricultural soils become increasingly relevant (Bol et al., 2018; Le Moal et al., 2019; Schoumans

et al., 2014). P retention and delivery to streams are closely linked to sorption in soils influenced by abiotic factors such as pH and redox conditions (Withers & Jarvie, 2008). Riparian wetlands are usually considered as sinks for agricultural P, but can also act as a source during rewetting after warm periods or under anoxic conditions (Dupas, Gruau, et al., 2015; Gu et al., 2017). For organic carbon, sources are linked to zones of organic matter accumulation, where biomass production exceeds removal via decomposition, such as in wetlands and peatlands (Clark et al., 2010). Riparian zones are important source areas for dissolved organic carbon (DOC) (Clark et al., 2010; Laudon et al., 2011; Musolff et al., 2018), which are usually hydrologically connected to the stream, whereas more distant DOC source areas might not intersect discharge generating zones (Bishop et al., 2004). Riparian zones are thus potential hot spots of biogeochemical processes, such as denitrification, DOC production and consumption and both P trapping and release, which are often linked to redox conditions and hence to water table dynamics. After the delivery to the stream, in-stream processes such as redox reactions and uptake can further remove, retain, transform or remobilize the nutrients before they reach the catchment outlet (Battin et al., 2008; Gomez-Velez et al., 2015).

Generally, the interplay between the solute source areas and hydrological connectivity has been found to be the major control of solute export dynamics (e.g., Herndon et al., 2015; Musolff et al., 2017; Seibert et al., 2009; Thompson et al., 2011; Tunaley et al., 2017). If solute source areas are uniformly distributed in a catchment, a chemostatic regime is established, as is typical for geogenic solutes (Thompson et al., 2011). Previous studies have found evidence that NO_3 often exhibits a chemostatic export regime in agricultural catchments (e.g., Basu et al., 2010, 2011; Dupas et al., 2016). This chemostatic regime is attributed to the built-up legacy of high N inputs in the past, causing spatial homogenization of sources (Basu et al., 2010; Thompson et al., 2011), which suggests a significant anthropogenic impact on NO_3 export dynamics. Similarly, excess P inputs have led to P legacies in soils and sediments (Jarvie et al., 2013; Schoumans et al., 2015; Sharpley et al., 2013). Legacy effects may hamper mitigation measures designed to reduce exported nutrient loads by dampening concentration responses and creating time lags up to several decades (Bouraoui & Grizzetti, 2011; Howden et al., 2010; Meals et al., 2010; Van Meter & Basu, 2015). In contrast, chemodynamic regimes are related to heterogeneously distributed source areas and variable discharge generating zones (Musolff et al., 2017; Zhi et al., 2019). Source heterogeneity can be linked, for example, to distinct production zones and the resulting vertical soil distribution profiles (Seibert et al., 2009), to vegetation and soil organic matter patterns (as shown for DOC by Herndon et al., 2015), and to heterogeneous land use patterns connected to inputs such as fertilizers (Musolff et al., 2017). Chemodynamic exports can also result from reactions along different flow paths. Flow paths with longer travel times, dominating during low flow conditions, are affected more than shorter ones. Thus removal along flow paths leads to depleted low-flow concentrations and thus enrichment patterns (Musolff et al., 2017) while production or accumulation processes lead to dilution patterns (Ameli et al., 2017; Musolff et al., 2017). Moreover, transient processes can cause temporal variations in source zones, for example long-term input changes from fertilizer applications (Ehrhardt et al., 2019) or temporally variable dissolution of accumulated phosphorus (Gu et al., 2017). However, spatial variability in export patterns of different archetypal catchments (catchments with different functioning) can collapse into a chemostatic downstream signal if concentrations vary asynchronously (Abbott et al., 2018). In summary, chemodynamic regimes signal variable combinations of discharge generating zones with different solute source strengths, travel times and reactivity along the flow paths within a catchment.

The anthropogenic impact on nutrient cycles and their effects on nutrient levels in streams (e.g., Gruber & Galloway, 2008; Hansen et al., 2018; Howden et al., 2010) as well as on nutrient export regimes have been discussed in several studies. However, to draw general and transferable conclusions a large sample size is required (Gupta et al., 2014). So far, only few studies consider a large number of catchments and different solutes (e.g., Basu et al., 2010; Moatar et al., 2017; Zarnetske et al., 2018). It thus remains uncertain how general and wide-spread the anthropogenic impact and resulting homogeneity or heterogeneity of sources is over a wide range of landscapes compared to natural controls, heterogeneity and reactivity (Ehrhardt et al., 2019; Van Meter & Basu, 2017). Therefore, we seek to understand (1) what drives nutrient concentration levels and dynamics across a large variety of catchments, and (2) how do anthropogenic impacts such as nutrient inputs interact with natural factors such as the hydroclimate, topography, and subsurface conditions. Our exploratory analysis is guided by the hypothesis that the differences of nutrient export dynamics

among catchments are dominantly controlled by the degree of spatial heterogeneity of diffuse sources, as opposed to geologic, climatic or topographic controls or the mere input load of nutrients to the catchment.

To this end, we analyze a newly assembled Germany-wide water quantity and quality data base (Musolff, 2020; Musolff et al., 2020). We use mean *C* and *C*-*Q* relationships of NO_3-N, PO_4-P and total organic carbon (TOC) to classify riverine nutrient dynamics in 787 independent catchments covering a wide range of ecoregions and large gradients in physical and hydroclimatic properties. We then disentangle the predictive role of anthropogenic and natural catchment properties to infer dominant controls and to hypothesize about the underlying processes by linking the descriptors to *C*-*Q* export metrics. Potential predictors include topography, land cover, geology, and hydroclimate, as well as diffuse and point sources and proxies for spatial source heterogeneity. Knowledge on dominant controls of nutrient export can serve to improve nutrient export models aiming at the catchment scale and to better tailor water quality management.

2. Materials and Methods

2.1. Water Quality and Quantity Data Set

Water quality data from river stations across Germany were gathered from the German federal state environmental authorities (Musolff, 2020; Musolff et al., 2020). The authorities regularly monitor the surface water quality in the context of the WFD (EEC, 2000), taking grab samples with a biweekly to seasonal frequency. Here, we focused on the three major nutrients: Nitrate-N concentrations as the dominant form of dissolved N (NO_3^--N), the biologically available dissolved orthophosphate phosphorus (PO_4^{3-}-P) and TOC concentrations. For brevity we use NO_3-N, PO_4-P without charges in the text. We used TOC instead of DOC because of better data availability and a strong correlation with a regression slope of about 0.87 between mean DOC and TOC concentrations (see Figure S1), and DOC representing about 81.3 (±7.9) % of TOC on average. Daily mean discharge time series at the water quality locations were partly provided together with the quality data (Musolff, 2020; Musolff et al., 2020).

Out of the initial pool of 6,000 sites of the newly assembled Germany-wide data base, water quality time series were selected based on the following criteria concerning the quality and availability of concentration and spatial data:

1) Data availability of at least three years in the target period from 2000 to 2015. This time period excludes major changes in the 1990s when major improvements of wastewater treatment were put into place (Westphal et al., 2019)
2) Minimum of 70 concentration samples after outlier removal. As the large number of sites demanded a cost-effective method, only extreme outliers likely to be typographical errors were removed (following Oelsner et al., 2017). We defined outliers as concentrations greater than mean $C + 4$*standard deviation in logarithmic space (confidence level >99.99% assuming lognormal distribution of concentrations) for all elements and as PO_4-P concentrations >100 mg l^{-1}, and TOC concentrations >1,000 mg l^{-1} in terms of absolute values
3) Seasonal coverage of the concentration data, that is the samples from all possible three consecutive months constitute at least 10% of the samples on average. This includes stations with data systematically missing in one month
4) Left-censored data of the concentration time series (values below the detection limit) must be less than 50% of the samples
5) Catchment area must be delineable from topography, that is we excluded stations with major deviations between location of real river network and topography-based basin area. The catchments were delineated based on flow accumulation derived from a digital elevation model (EEA, 2013) of 25 m resolution resampled to 100 m and the river network from the CCM River and Catchment Database (version 2.1, De Jager & Vogt, 2007), with some manual adaptations of river segments which drastically improve the match between catchments and the real river network

6) Independence of catchments, which was defined as nested catchments sharing less than 20% of their catchment area with any upstream station
7) Station must not be directly located at the outlet of a reservoir or lake (about 5 km), because the water quality in the vicinity of a lake or reservoir is expected to be mainly a result of lake dynamics, thus likely masking the effect of catchment processes
8) Data availability of catchment characteristics. This leads to the criterion that a minimum of 70% of the catchment area must fall within the borders of Germany, as some of the geodata were limited to Germany, such as N-surplus and point sources (see Section 2.3)

Applying the above criteria resulted in a set of 787 catchments with 759 NO_3-N, 695 PO_4-P, and 722 TOC time series. At 278 sites out of those catchments, observed discharge data were available. Altogether, the analyzed data base consists of a total of 110,603 concentration samples for combinations of dates and locations with an average between 135 (TOC) and 142 (NO_3-N) samples per site (from 2000 to 2015).

2.2. Metrics of Water Quality Dynamics

We used arithmetic mean concentrations and metrics of the *C*-*Q* relationships to characterize the nutrient concentration levels and dynamics in the different catchments. Before calculating basic statistics at each station, that is mean concentrations and the standard deviation, we replaced the concentration values falling below the detection limit (left-censored data) with half of the detection limit (see e.g., Hunsaker & Johnson, 2017; Underwood et al., 2017).

The relationship between concentration (C) and discharge (Q) can be described as: $\log(C) = \log(a) + b\log(Q) + \varepsilon$ with ε as a normal-distributed error term (Vogel et al., 2005). As described by Godsey et al. (2009), we fit the model without an error term (equals power law relationship $C = aQ^b$) to estimate the parameter slope b for each station, separately. Slope b characterizes the export pattern of a constituent such that $b > 0$ indicates an enrichment pattern, $b < 0$ a dilution pattern, while $b \approx 0$ describes a non-significant, neutral *C*-*Q* pattern (Musolff et al., 2017). Thompson et al. (2011) note that the power law *C*-*Q* model and metrics as R^2 and *f*-statistics become uninformative when b approaches zero. The separation of the three export pattern classes is therefore based on the significant difference of the slope b from zero (*t*-test, 95% confidence level). We consider this approach as an alternative to a classification based on fixed ranges of slope b (M. Botter et al., 2020; Herndon et al., 2015; Zimmer et al., 2019). We excluded left censored values (below the detection limit) from the regression analysis and limited the censored fraction to 20% assuming that otherwise parts of the *C*-*Q* relationship could be underrepresented.

We aggregated low-frequency data over different seasons and hydroclimatic conditions to obtain general *C*-*Q* relationships. Generally, ambivalent *C*-*Q* relationships can cause dispersion in regression estimates toward increased chemostatic export (Burns et al., 2019; Minaudo et al., 2019). Several studies have therefore applied models deviating from a simple power-law *C*-*Q* relationship (Minaudo et al., 2019; Moatar et al., 2017; Underwood et al., 2017). In several catchments, segmented models yielded better performances than the simple power-law (Diamond & Cohen, 2018; Marinos et al., 2020). However, the direction of segmented *C*-*Q* relationships rarely changed, for example from upward to downward (Moatar et al., 2017), which suggests that the general behavior of slope b can be preserved in a simple power law approach. To further test if a single power law was justified for our case domain, we compared the simple (power law) model to segmented regression models in log space using the Akaike information criterion (Akaike, 1974) as presented by Marinos et al. (2020). A single power law was superior in about 75% of the study catchments (Table S1), that is an increase in model complexity was not justified. In the other 25% of the study catchments, we noticed on average an increase in the R^2 by 10%. Based on these results and for the sake of consistency across the study catchments, we selected the parsimonious single power law model for further investigations.

Additionally, we used the ratio of the coefficients of variation of concentration and discharge CV_C/CV_Q to characterize export regimes (Thompson et al., 2011). The export regime is considered as chemostatic for small CV_C/CV_Q (<0.5) and as chemodynamic for high CV_C/CV_Q (Musolff et al., 2015).

The combination of both statistics (slope b and CV_C/CV_Q) leads to six distinct C-Q export classes (Figure S2) characterizing the distinct combinations of chemostatic and chemodynamic regimes within the different export patterns. This distinction is especially important for non-significant C-Q relationships ($b \approx 0$), which can still demonstrate a chemodynamic export with C variability ($CV_C/CV_Q \geq 0.5$) related to other factors than Q. Such dynamics can result from highly reactive export such as fast turnover in the streams (Musolff et al., 2015). Differences in mean concentrations between the export patterns and regimes were tested for significance ($\alpha = 0.05$) using a Kruskal-Wallis rank sum test. In case of significant differences between the C-Q patterns, the Wilcoxon rank sum test was used for pairwise comparisons to identify the difference in patterns.

2.3. Catchment Characteristics

The 278 C-Q catchments with available discharge data cover 43.7% of Germany, while the 787 C catchments cover 65.6%. Catchment sizes vary from 1.9 to 77,099.2 km^2 (4.4–23,162.7 km^2 for C-Q catchments), with 50% of the catchments smaller than 97.1 km^2 (<235.6 km^2) and 95% < 1,257.4 km^2 (<2,540.0 km^2). The catchments intersect all ten hydrogeological regions in Germany (BGR & SGD, 2015) and span a wide range of topographical, hydroclimatic, lithological and soil properties with varying anthropogenic presence. A summary of catchment characteristics is given in Table 1 and represented distributions of selected characteristics (matching mean conditions in Germany) are shown in Figure 1. The catchment characteristics are provided in a data repository (Ebeling, 2021a). The selection of catchment characteristics was inspired by several previous studies (e.g., G. Botter et al., 2013; Dupas, Delmas, et al., 2015; Moatar et al., 2017; Musolff et al., 2018, 2015; Onderka et al., 2012) and limited by data availability over the large scale.

In addition to climatic characteristics available for all catchments, hydrological characteristics were calculated for a smaller subset of catchments where daily discharge measurements were available ($n = 186$). The hydrological variables included mean discharge, mean specific discharge, runoff coefficient, seasonal ratio, base-flow index (BFI, WMO, 2008) and flashiness index based on flow percentiles following Jordan et al. (2005) (for details see Tables S2 and S9–S911).

To test our main hypothesis over a wide range of catchments, we parameterized source heterogeneity from landscape characteristics. Inspired by Musolff et al. (2017), who found "structured heterogeneity"—defined as nonlinear correlation between source concentration and travel time—to dominantly shape C-Q relationships, we aim at connecting discharge generating zones (implicitly related to travel times and water ages) with source distributions. Thereby, we focused on parameterizing the prevailing structured heterogeneity in each catchment as opposed to random variability and considered both horizontal and a vertical parameterization component as visualized in the supporting information (Figure S3).

For the horizontal component of source heterogeneity of diffuse NO_3-N and PO_4-P sources, we assumed horizontal flow distances from the solute source to the stream network to link to flow paths and thus travel times. Horizontal source heterogeneity is considered as a temporally invariant catchment characteristic and does not account for seasonal or short term variability of nutrient availability within the source but rather represents the catchment setup with regards to spatial land use arrangement. Agricultural diffuse nutrient source areas were defined as seasonal, perennial cropland and grassland estimated based on a highly resolved land use map of 2015 (Pflugmacher et al., 2018). We computed horizontal flow distances along the topographic flow direction toward the stream using the ESRI ArcGIS (version 10.6). The stream grid was derived from the EU-wide EU-Hydro river network (EEA, 2016b). Based on the flow distance grid, we resampled the land cover map with a 30 m resolution to 100 m using the majority method. For each catchment, we then estimated the mean agricultural source area distance to nearest stream (sdist_mean) and the fraction of agricultural source area within classes of flow distances of 400 m each. Subsequently, we fitted a linear regression to the class values of the histogram weighted by the corresponding class frequencies within the catchment. When the slope of this regression is positive (het_h > 0), source areas tend to be located further from the stream, whereas when it is negative (het_h < 0), sources tend to be closer and sources are homogeneously distributed when het_h = 0 (Figure S3). As the EU-Hydro river network partly deviates from delineated catchments and contains different degrees of details, 78 C and 38 C-Q catchments (mostly small ones) resulted in implausible distance distributions. Therefore, het_h was assigned as missing value

Table 1
Catchment Descriptors Used in the Analysis, Associated Methods and Data Sources

Category	Variable	Unit	Description and method	Data source
Topography	area	km^2	Catchment area	
	dem_mean	mamsl	Mean elevation of catchment, from DEM (digital elevation model) rescaled from 25 to 100 m resolution using average	EEA, 2013
	slope_mean	°	Mean topographic slope of catchment, from DEM	EEA, 2013
	twi_mean	–	Mean topographic wetness index (TWI, Beven & Kirkby, 1979)	EEA, 2013
	twi_90p	–	90th percentile of the TWI as a proxy for riparian wetlands (following Musolff et al., 2018)	EEA, 2013
	drain_dens	km^{-1}	Average drainage density of the catchment. Gridded drainage density is provided as the length of surface waters (rivers and lakes) per area from a 75 km^2 circular area around each cell center	BMU, 2000
Land cover	f_urban	–	Fraction of artificial land cover	EEA, 2016a
	f_agric	–	Fraction of agricultural land cover	EEA, 2016a
	f_forest	–	Fraction of forested land cover	EEA, 2016a
	f_wetland	–	Fraction of wetland cover	EEA, 2016a
	f_water	–	Fraction of surface water cover	EEA, 2016a
	p_dens	inhabitants km^{-2}	Mean population density	CIESIN, 2017
Nutrient sources	N_surp_00	kg N ha^{-1} y^{-1}	Mean nitrogen surplus per catchment during sampling period (2000–2015) including N surplus on agricultural land and atmospheric deposition on non-agricultural areas	Bach et al., 2016; Häußermann et al., 2019
	N_surp_80	kg N ha^{-1} y^{-1}	Mean N surplus per catchment before and during sampling period (1980–2015) to consider historic (legacy) inputs	Bach et al., 2016; Häußermann et al., 2019
	N_WW	kg N ha^{-1} y^{-1}	Sum of N input from point sources including waste water treatment plants (WWTP) > 2000 person equivalents from the database of the European Environment Agency covering areas beyond Germany and data collected from 13 federal German states covering smaller WWTP within Germany	Büttner, 2020a, 2020b
	P_WW	kg P ha^{-1} y^{-1}	Sum of P input from WWTP analogous to N_WW	Büttner, 2020a, 2020b
	het_h	–	Slope of relative frequency of source areas in classes of flow distances to stream as a proxy for horizontal source heterogeneity (see in text Section 2.3)	Source areas based on Pflugmacher et al., 2018
	sdist_mean	m	Mean lateral flow distance of source areas to stream (see in text Section 2.3)	Source areas based on Pflugmacher et al., 2018
	het_v	–	Mean ratio between potential seepage and groundwater NO_3-N concentrations as proxy for vertical concentration heterogeneity (see in text Section 2.3)	Knoll et al., 2020
Lithology and soils	f_calc	–	Fraction of calcareous rocks	BGR & UNESCO (eds.), 2014
	f_calc_sed	–	Fraction of calcareous rocks and sediments	BGR & UNESCO (eds.), 2014
	f_magma	–	Fraction of magmatic rocks	BGR & UNESCO (eds.), 2014
	f_metam	–	Fraction of metamorphic rocks	BGR & UNESCO (eds.), 2014
	f_sedim	–	Fraction of sedimentary aquifer	BGR & UNESCO (eds.), 2014
	f_silic	–	Fraction of siliciclastic rocks	BGR & UNESCO (eds.), 2014
	f_sili_sed	–	Fraction of siliciclastic rocks and sediments	BGR & UNESCO (eds.), 2014
	dtb	cm	Median depth to bedrock in the catchment	Shangguan et al., 2017
	f_gwsoils	–	Fraction of water-impacted soils in the catchment (from soil map 1:250,000), including stagnosols, semi-terrestrial, semi-subhydric, subhydric and moor soils	BGR, 2018

Table 1
Continued

Category	Variable	Unit	Description and method	Data source
	f_sand	–	Mean fraction of sand in soil horizons of the top 100 cm	FAO/IIASA/ISRIC/ISSCAS/JRC, 2012
	f_silt	–	Mean fraction of silt in soil horizons of the top 100 cm	
	f_clay	–	Mean fraction of clay in soil horizons of the top 100 cm	
	water_root	mm	Mean available water content in the root zone from pedo-transfer functions	Livneh et al., 2015; Samaniego et al., 2010; Zink et al., 2017
	theta_S	–	Mean porosity in catchment from pedo-transfer functions	Livneh et al., 2015; Samaniego et al., 2010; Zink et al., 2017
	soil_N	g kg^{-1}	Mean top soil N in catchment	Ballabio et al., 2019
	soil_P	mg kg^{-1}	Mean top soil P in catchment	Ballabio et al., 2019
	soil_CN	–	Mean top soil C/N (Carbon/Nitrogen) ratio in catchment	Ballabio et al., 2019
Climate	P_mm	mm	Mean annual precipitation (period 1986–2015 used for all climatic variables)	Cornes et al., 2018
	P_SIsw	–	Seasonality of precipitation as the ratio between mean summer (Jun-Aug) and winter (Dec-Feb) precipitation	Cornes et al., 2018
	P_lambda	–	Mean precipitation frequency λ as used by G. Botter et al., 2013	Cornes et al., 2018
	PET_mm	mm	Mean potential evapotranspiration	Cornes et al., 2018
	AI	–	Aridity index as AI = PET_mm/P_mm	Cornes et al., 2018
	T_mean	°C	Mean annual air temperature	Cornes et al., 2018

in catchments without intersection with any river segment or a maximum flow distance to stream ≥15 km. We do not expect that results are generally influenced by this limitation as the remaining catchments still represent well the parameter space. However, these missing values lower the sample size, the related variables (het_h and sdist_mean) did not rank among the dominant predictors, nor did they improve model performances; het_h and sdist_mean were therefore excluded from the main analysis (Section 3.3). Results corresponding to the smaller subset including het_h and sdist_mean are presented in the supporting information (Tables S4 and S5).

Similar to the horizontal source heterogeneity, we parameterized the vertical concentration heterogeneity as concentration gradients over depth. We again assume a link between flow paths over depth and travel times. For each catchment, we calculated the mean of the ratio between the potential seepage NO_3 concentrations and groundwater NO_3 concentrations (Figure S3). This ratio resembles the parameter C_{ratio} of soil versus groundwater concentrations used in Zhi et al. (2019). We used the groundwater NO_3 and potential seepage concentrations across Germany presented by Knoll et al. (2020). They estimated groundwater NO_3 concentrations with a resolution of 1 km using a random forest model trained on observed groundwater concentrations (averages over the years 2009–2018) and spatial predictors. Mean groundwater NO_3 concentrations from Knoll et al. (2020) correlated positively with mean riverine NO_3 concentrations in our study ($r = 0.73$) and with average low-flow NO_3 concentrations ($r = 0.63$ for all observations with daily Q below the 10th percentile). The potential seepage NO_3 concentrations (Knoll et al., 2020) were calculated as a ratio of N surplus (Bach et al., 2016; Häußermann et al., 2019) and the seepage rate (BGR, 2003). We note that this approach does not estimate the actual but a potential seepage concentration, as we do not consider denitrification and lateral NO_3 fluxes in the unsaturated zone. This implies that het_v integrates removal processes across both the unsaturated and the saturated zone. Due to data availability, vertical heterogeneity parameterization was calculated for NO_3 only.

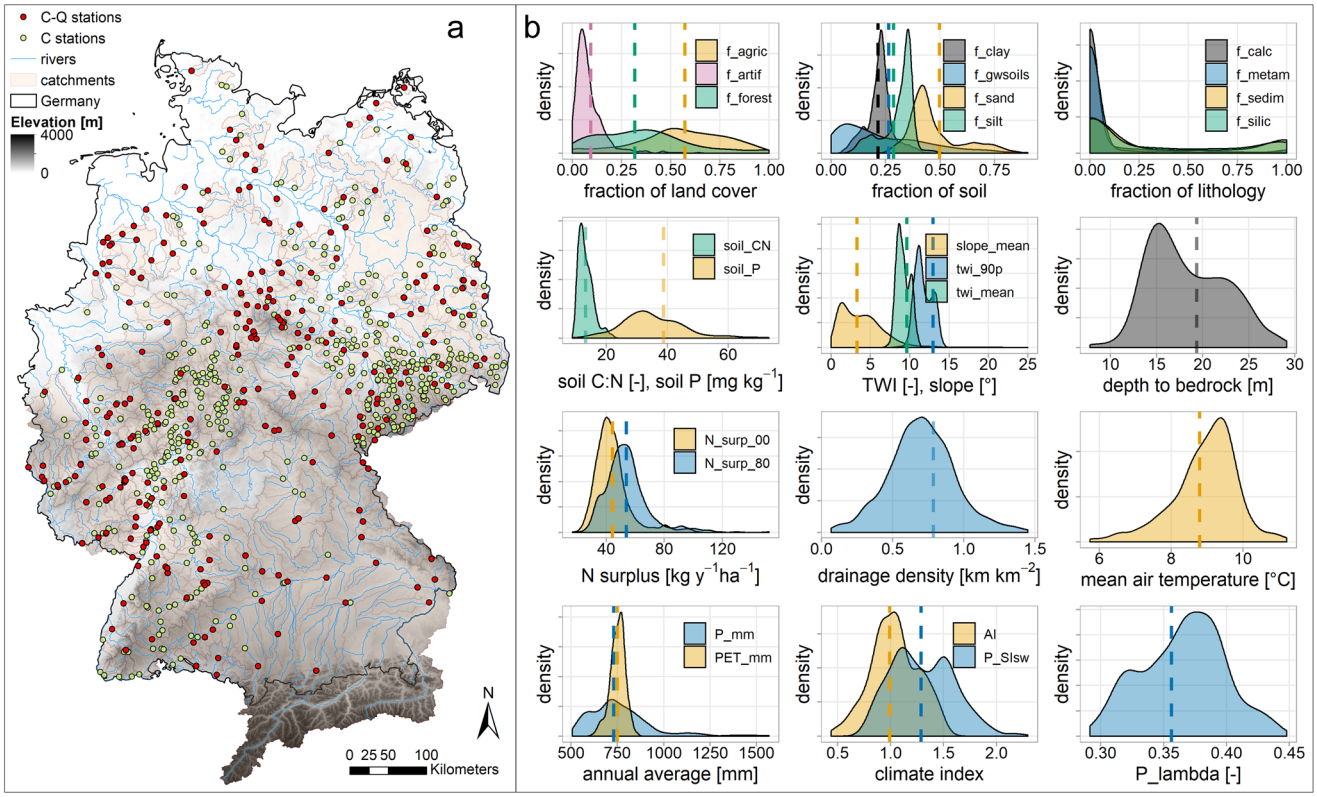

Figure 1. The study area with stations of concentration (*C*) and additional discharge (*C*-*Q*) data and corresponding catchments overlaying elevation (a) and distributions of selected catchment characteristics represented by the *C* catchments (b). TWI, topographic wetness index; P_mm, precipitation; PET_mm, potential evapotranspiration; AI, aridity index; P_SIsw, precipitation seasonality; P_lambda, precipitation frequency. Refer to Table 1 for detailed explanations of the parameters. Vertical dashed lines mark corresponding average values for Germany.

2.4. Linking Water Quality Metrics to Descriptors

Rank-based correlations provide a first indication of existing links between the individual catchment descriptors and the response metrics (Figure S5). Yet, due to inter-correlations among several descriptors (Figure S4), suitable multivariable statistical approaches are required for a proper interpretation of linkages and hierarchies.

We applied Partial Least Squares Regressions (PLSR, Wold et al., 2001) in combination with the Variable Influence of Projection (VIP, Wold et al., 2001) and Random Forests (RF, Breiman, 2001) to identify controls for differences in mean concentrations, export patterns and regimes of NO_3-N, PO_4-P and TOC among the studied catchments. Both PLSR and RF can handle co-linear descriptors as given here and provide variable importance measures to rank descriptors and interpret dominant controls. Still, ambiguity in certain predictors can limit clear linking of the identified dominant controls to drivers and processes. Both models have been applied in water quality studies, for example PLSR for investigating solute export and their predictors (Musolff et al., 2015; Onderka et al., 2012; Wallin et al., 2015) and RF for estimating the spatial distributions of groundwater NO_3 concentrations (Knoll et al., 2019; Ouedraogo et al., 2019; Rodriguez-Galiano et al., 2014) and artificial drainage systems (Møller et al., 2018). While PLSR is based on linear relationships, RF is a non-linear method. Here, we combine the two approaches as a model ensemble to address the uncertainty of data-driven analyses and thus to increase the robustness and interpretability of the results (Schmidt et al., 2020).

One PLSR and one RF model per response variable were set up using the catchment characteristics as descriptors (Table 1, excluding sdist_mean and het_h). In addition, models including either sdist_mean and

Table 2
Summary Statistics of the Calculated Metrics of Concentration (C) and Concentration-Discharge (C-Q) Relationships

	Concentration				*C-Q* relationships		
	n *C*-catchments with <50% censored data	Mean [mg l^{-1}]	Median [mg l^{-1}]	CV_C	*n* *C-Q*-catchments with <50% (<20%) censored data	CV_C/CV_Q	*b*
NO_3-N	759	4.06 ± 2.69 (3.71 ± 3.14)	3.86 ± 2.74 (3.4 ± 3.2)	0.38 ± 0.27 (0.29 ± 0.27)	275 (274)	0.47 ± 0.43 (0.33 ± 0.34)	0.26 ± 0.35 (0.16 ± 0.36)
PO_4-P	695	0.12 ± 0.12 (0.08 ± 0.11)	0.10 ± 0.10 (0.07 ± 0.09)	0.68 ± 0.33 (0.60 ± 0.28)	261 (236)	0.70 ± 0.42 (0.58 ± 0.31)	−0.22 ± 0.27 (−0.25 ± 0.35)
TOC	722	5.88 ± 2.96 (4.96 ± 3.35)	5.33 ± 2.81 (4.45 ± 3.19)	0.41 ± 0.16 (0.38 ± 0.17)	256 (255)	0.49 ± 0.33 (0.40 ± 0.23)	0.18 ± 0.22 (0.14 ± 0.23)

Note. Given are the sample size *n* and the mean ± standard deviation of the mean and median concentrations, the coefficients of variation of concentration CV_C and the metrics of *C-Q* relationships (i.e. CV_C/CV_Q, slope *b*). Values in brackets refer to median ± interquartile range.

het_h or hydrological descriptors were run for a smaller number of catchments (due to missing values, Tables S4 and S5). Nutrient-specific point sources were considered only for the corresponding nutrient (i.e., either NO_3-N or PO_4-P). Since for diffuse sources, only N surplus but no P surplus data were available, the former was used as a descriptor for all nutrients because of expected correlations to P surplus (Dupas, Delmas, et al., 2015; Minaudo et al., 2019). N surplus was thus considered as a proxy for agricultural, diffuse P inputs together with the topsoil P content, which also correlate positively ($r = 0.52$ for N_surp_80, Figure S4). All data were standardized to unit variance and zero mean to give the variables the same prior importance and enhance the model stability (Wold et al., 2001). Yeo-Johnson transformations did not change results. Furthermore, we used simple and multiple linear regressions for selected descriptors as parsimonious models to complement the complex PLSR and RF models.

To assess the model performances and to tune the number of components in PLSR, we conducted a three times repeated 10-fold cross-validation (Table S3). The variable importance in RF was assessed based on the mean increase of accuracy based on "out-of-bag" (OOB) samples. The analysis was conducted in *R* (version 3.5.0, Team, 2019) with the *caret* package (version 6.0–84, Kuhn et al., 2019) and partial dependence plots created with the *pdp* package (version 0.7.0., Greenwell, 2017).

For our analyses, we assume stationary general catchment functioning over the analyzed time period (2000–2015). Even if this may not be true in all cases, integrating over this relatively short period should be acceptable and not corrupt the generally observed relationships.

3. Results

3.1. Classification of *C-Q* Metrics and Mean Concentrations

Basic statistics of the catchments' mean concentrations and *C-Q* metrics are given in Table 2. Overall, the averages of mean concentrations over the studied catchments were 4.06 mg l^{-1} NO_3-N, 0.12 mg l^{-1} PO_4-P, and 5.88 mg l^{-1} TOC. The average coefficient of variation of concentration CV_C varied between 0.38 for NO_3-N, 0.41 for TOC, and 0.68 for PO_4-P. In general, *C-Q* metrics covered all types of patterns and regimes, with mean slope $b > 0$ and mean $CV_C/CV_Q < 0.5$ for NO_3-N and TOC and mean slopes $b < 0$ and mean $CV_C/CV_Q > 0.5$ for PO_4-P, while standard deviations of *b* were larger than absolute mean *b* for all nutrients. The *C-Q* power-law regressions showed similar model performances for the three nutrients with mean $R^2 = 0.27 \pm 0.24$ for NO_3-N slightly higher than PO_4-P ($R^2 = 0.21 \pm 0.19$) and TOC ($R^2 = 0.19 \pm 0.20$).

For NO_3-N export, the majority of catchments showed a chemostatic regime (74%, $n = 200$) and an enrichment pattern (69%, $n = 188$), while 45% combined both (Figures 2a and 2b). Highest mean concentrations

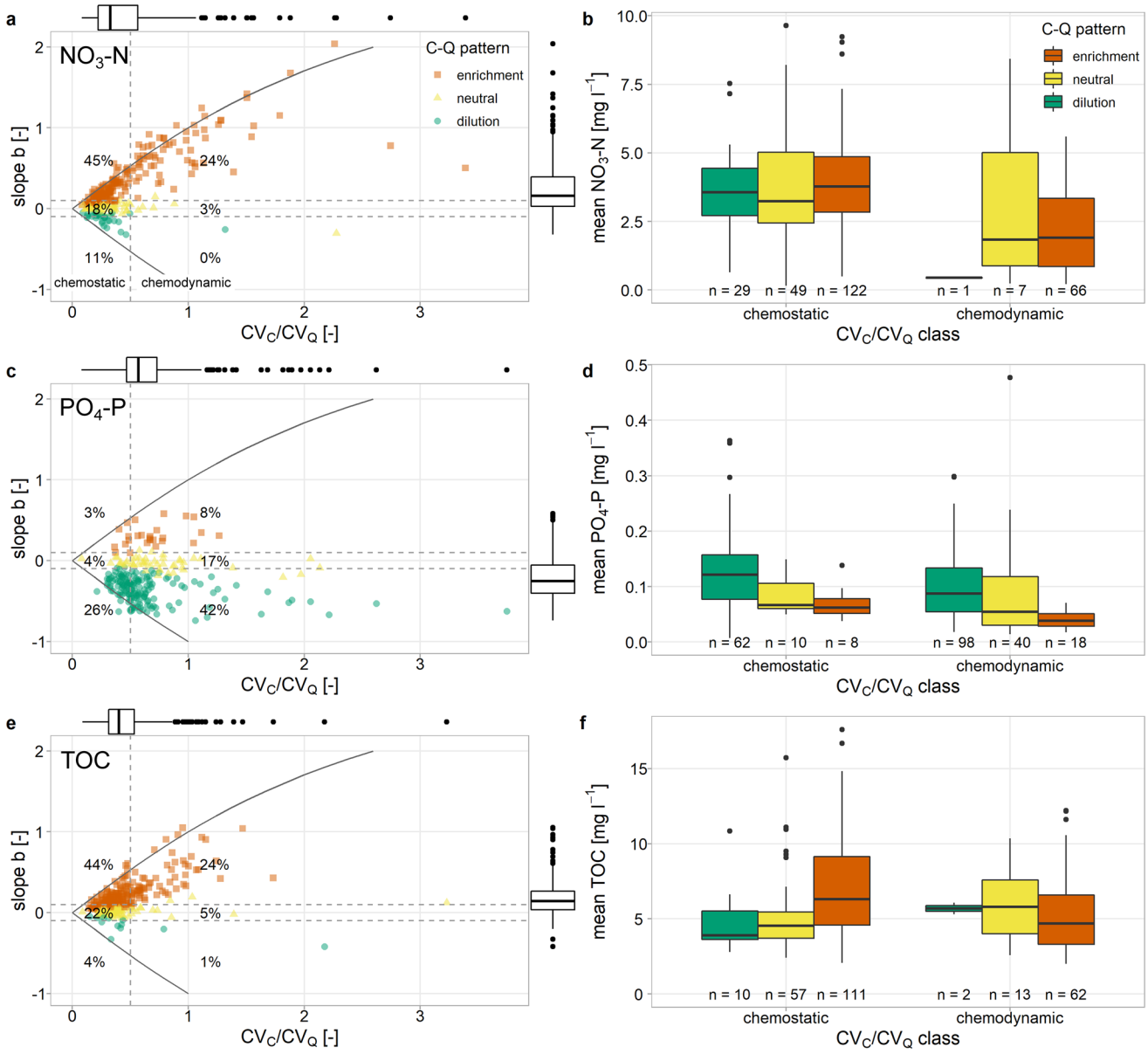

Figure 2. *C-Q* classification schemes composed of CV_C/CV_Q for export regimes and slope *b* for export patterns for NO_3-N (a), PO_4-P (c) and TOC (e), scheme adapted from Musolff et al. (2015). Colors and shape indicate the class of *C-Q* patterns, horizontal dashed lines approximate these class divisions, while the vertical dashed line divides the two classes of *C-Q* regimes with $CV_C/CV_Q < 0.5$ for chemostatic and $CV_C/CV_Q > 0.5$ for chemodynamic regimes. The solid lines indicate the theoretical boundaries between slope *b* and CV_C/CV_Q for $CV_Q = 0.6$ (after Musolff et al., 2015). Percentages indicate the portion of catchments assigned to the corresponding *C-Q* class. Mean concentrations of NO_3-N (b), PO_4-P (d) and TOC (f) are shown as boxplots for each class. n, number of observations in this class.

were observed for chemostatic regimes, while mean concentrations of the group with chemodynamic regimes were significantly lower (Kruskal-Wallis, $p < 0.001$). The mean concentrations between the different *C-Q* patterns did not differ significantly.

For PO_4-P export, the majority of catchments exhibited a chemodynamic regime (67%, $n = 156$) and a dilution pattern (68%, $n = 160$), while the combination of both can be found for 42% of all catchments (Figures 2c and 2d). Independent of the *C-Q* pattern, mean concentrations were significantly lower in the chemodynamic compared to the chemostatic regime (Kruskal-Wallis, $p < 0.001$). Among the *C-Q* patterns,

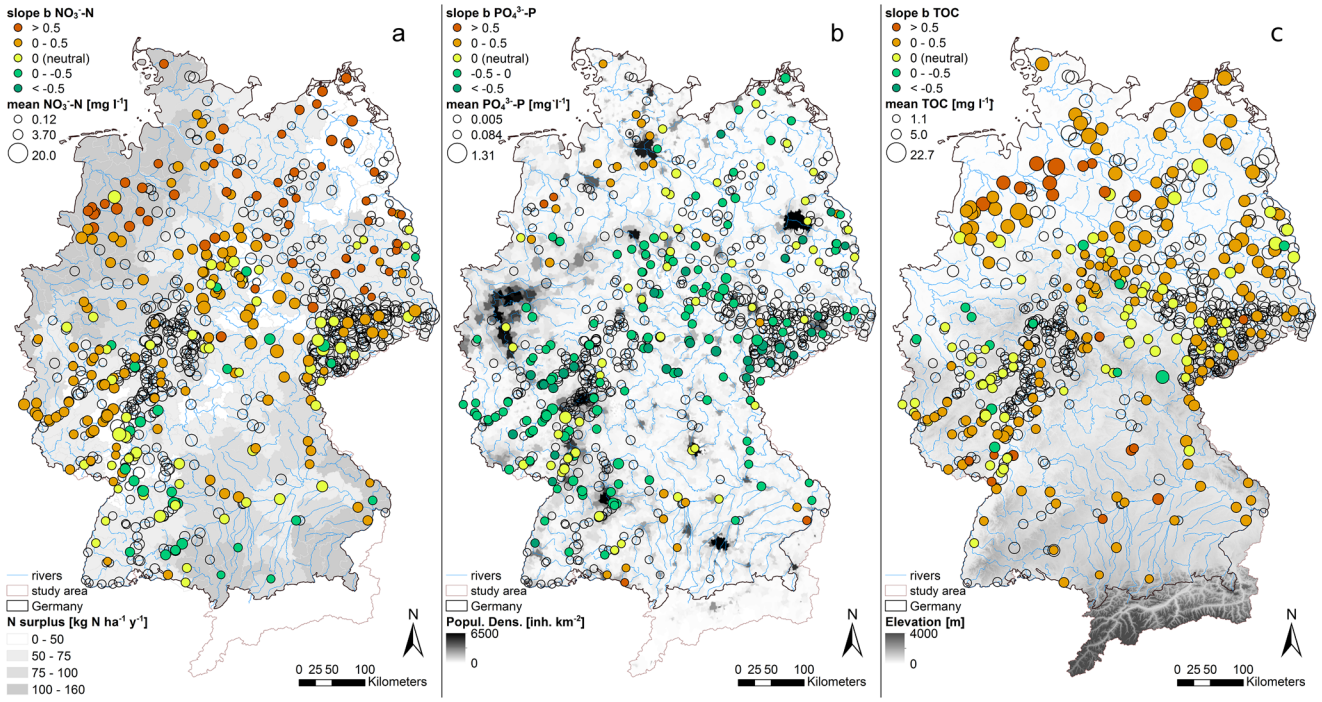

Figure 3. Spatial patterns of *C-Q* slope *b* and mean concentrations across Germany (a) for NO_3-N with average N surplus from 2000 to 2015 on county level (Bach et al., 2016; Häußermann et al., 2019), (b) PO_4-P with population density, and (c) TOC with the elevation as base map. Point size represents mean concentrations, scaled to the respective range across the study catchments with minimum, mean and maximum shown in the legend.

mean concentrations were significantly higher for dilution patterns compared to neutral patterns (Wilcoxon, $p = 0.002$) and to enrichment patterns (Wilcoxon, $p < 0.001$). Catchments with enrichment patterns showed the lowest mean concentrations, though they were not significantly different from catchments with neutral *C-Q* patterns (Wilcoxon, $p = 0.057$).

For TOC, chemostatic export (70%, $n = 178$) and enrichment patterns (68%, $n = 173$) prevailed, with 44% of the catchments combining both (Figures 2e and 2f). Overall, the chemostatic regime showed significantly higher mean TOC concentrations than the chemodynamic regimes (Kruskal-Wallis, $p = 0.014$). The mean concentrations between the *C-Q* patterns also differed significantly (Kruskal-Wallis, $p = 0.007$). The catchments with enrichment patterns had significantly higher mean concentrations than those exhibiting neutral *C-Q* patterns (Wilcoxon, $p = 0.011$), which was mainly apparent within the chemostatic regime (Figure 2f).

3.2. Spatial Patterns of Concentrations and Export Dynamics

The spatial organization of mean concentrations and export patterns of each nutrient are shown in Figure 3. Regional clusters of the export patterns can be observed for all nutrients. NO_3-N showed the strongest enrichment patterns in northern Germany and some dilution patterns in southern and southwestern Germany. The highest mean NO_3-N concentrations were found in the eastern part of Germany. For PO_4-P, dilution and neutral patterns prevailed in central, northeastern and southwestern Germany whereas the few enrichment patterns clustered in the northwest and southeast of Germany. Highest mean PO_4-P concentrations were found in central Germany, though a general spatial organization was not obvious for this metric. TOC also showed strong enrichment patterns in northern Germany, especially in the northwest, but also in the south of Germany, whereas the small number of dilution patterns seemed to cluster more in the west. The highest mean TOC concentrations were found in the lowlands in northern, esp. northwestern Germany, coinciding with the enrichment patterns.

Table 3
Ranked Drivers and Model Performances of PLSR With VIP and RF for the Three Nutrients and Metrics

Res-ponse	Mean concentration				*b*				CV_C/CV_Q			
NO_3-N	$n = 759$				$n = 274$				$n = 275$			
	PLSR		**RF**		**PLSR**		**RF**		**PLSR**		**RF**	
	$R^2_{CrossVal} = 0.64$		$R^2_{CrossVal} = 0.69$		$R^2_{CrossVal} = 0.57$		$R^2_{CrossVal} = 0.64$		$R^2_{CrossVal} = 0.60$		$R^2_{CrossVal} = 0.65$	
	$R^2_{train} = 0.66$		$R^2_{OOB} = 0.68$		$R^2_{train} = 0.57$		$R^2_{OOB} = 0.59$		$R^2_{train} = 0.58$		$R^2_{OOB} = 0.56$	
	Variable	**VIP**	**Variable**	**Imp**	**Variable**	**VIP**	**Variable**	**Imp**	**Variable**	**VIP**	**Variable**	**Imp**
	f_forest	1.93 (−)	f_forest	20.3	het_v	1.66 (+)	slope_mean	11.5	het_v	1.70 (+)	het_v	10.2
	f_agric	1.88 (+)	P_mm	17.4	twi_mean	1.55 (+)	twi_mean	11.2	f_sedim	1.58 (+)	twi_mean	9.3
	soil_CN	1.82 (−)	P_SIsw	16.2	dtb	1.48 (+)	dem_mean	9.0	dtb	1.42 (+)	slope_mean	9.3
	het_v	1.40 (−)	f_sedim	15.8	f_sedim	1.48 (+)	soil_N	8.1	f_silt	1.40 (−)	dem_mean	7.4
	f_sand	1.38 (+)	het_v	14.4	twi_90p	1.47 (+)	PET_mm	7.7	twi_mean	1.37 (+)	f_sedim	6.9
	f_clay	1.32 (+)	f_agric	13.9	dem_mean	1.46 (−)	P_mm	7.3	f_sand	1.36 (+)	soil_N	6.6
PO_4-P	$n = 695$				$n = 236$				$n = 261$			
	PLSR		**RF**		**PLSR**		**RF**		**PLSR**		**RF**	
	$R^2_{CrossVal} = 0.34$		$R^2_{CrossVal} = 0.40$		$R^2_{CrossVal} = 0.43$		$R^2_{CrossVal} = 0.47$		$R^2_{CrossVal} = 0.16$		$R^2_{CrossVal} = 0.21$	
	$R^2_{train} = 0.32$		$R^2_{OOB} = 0.30$		$R^2_{train} = 0.52$		$R^2_{OOB} = 0.48$		$R^2_{train} = 0.15$		$R^2_{OOB} = 0.09$	
	Variable	**VIP**	**Variable**	**Imp**	**Variable**	**VIP**	**Variable**	**Imp**	**Variable**	**VIP**	**Variable**	**Imp**
	P_WW	2.04 (+)	P_WW	23.1	N_surp_00	1.82 (+)	f_sedim	15.0	f_sedim	1.79 (+)	T_mean	6.8
	f_artif	1.71 (+)	dem_mean	9.2	N_surp_80	1.73 (+)	N_surp_00	13.1	f_sand	1.58 (+)	thetaS	5.8
	soil_CN	1.67 (−)	f_silt	8.9	f_sedim	1.61 (+)	N_surp_80	12.7	het_v	1.55 (+)	twi_mean	5.6
	pdens	1.60 (+)	PET_mm	8.2	twi_90p	1.36 (+)	P_lambda	9.3	dtb	1.54 (+)	WaterRoots	5.5
	PET_mm	1.53 (+)	f_silic	7.4	soil_P	1.35 (+)	twi_90p	9.2	f_silt	1.51 (−)	dem_mean	5.2
	f_sand	1.53 (−)	dtb	7.3	P_mm	1.35 (+)	P_SIsw	8.6	f_water	1.44 (+)	slope_mean	4.7
TOC	$n = 722$				$n = 255$				$n = 256$			
	PLSR		**RF**		**PLSR**		**RF**		**PLSR**		**RF**	
	$R^2_{CrossVal} = 0.61$		$R^2_{CrossVal} = 0.68$		$R^2_{CrossVal} = 0.19$		$R^2_{CrossVal} = 0.28$		$R^2_{CrossVal} = 0.15$		$R^2_{CrossVal} = 0.21$	
	$R^2_{train} = 0.62$		$R^2_{OOB} = 0.65$		$R^2_{train} = 0.26$		$R^2_{OOB} = 0.26$		$R^2_{train} = 0.23$		$R^2_{OOB} = 0.11$	
	Variable	**VIP**	**Variable**	**Imp**	**Variable**	**VIP**	**Variable**	**Imp**	**Variable**	**VIP**	**Variable**	**Imp**
	twi_90p	1.71 (+)	dem_mean	14.2	N_surp_00	1.55 (+)	f_sedim	11.8	f_sedim	1.43 (+)	drain_dens	8.9
	twi_mean	1.71 (+)	slope_mean	13.1	N_surp_80	1.46 (+)	N_surp_00	10.9	f_silic	1.36 (−)	f_calc	8.5
	f_sedim	1.57 (+)	twi_mean	13.1	f_sedim	1.43 (+)	N_surp_80	8.6	soil_N	1.34 (−)	f_silt	7.7
	slope_mean	1.46 (−)	twi_90p	12.0	f_silic	1.37 (−)	dem_mean	8.3	f_calc	1.33 (+)	P_SIsw	7.1
	dem_mean	1.37 (−)	PET_mm	11.0	het_v	1.27 (−)	f_silt	8.0	T_mean	1.33 (+)	soil_P	5.8
	dtb	1.36 (+)	f_sedim	9.9	AI	1.18 (−)	P_mm	7.8	f_gwsoils	1.31 (−)	P_mm	5.6

Note. Only the six highest ranked variables are shown; the complete results are given in Tables S6–S8 in the supporting information. CrossVal, cross-validation; OOB, out-of-bag samples; LSR, partial least squares regressions; RF, random forests; VIP, variable influence on projection of PLSR; Imp, variable importance in RF models.

3.3. Linking Water Quality Metrics to Catchment Characteristics

The variability in the *C*-*Q* metrics could be partly explained by the catchment characteristics, albeit not for all investigated nutrients and metrics (Table 3 and Figure S6). The average model performances from cross validation $R^2_{CrossVal}$ varied between 15.0% (PLSR for CV_C/CV_Q of TOC) and 69.2% (RF for mean NO_3-N). The $R^2_{CrossVal}$ were consistently higher for the RF models (on average 5.9%), however, the variance between the folds is high. The standard deviations of $R^2_{CrossVal}$ differed largely between models; they were lowest for

mean NO_3-N and mean TOC concentrations (7.3%–9.6%) and highest for slope *b* of TOC in RF (19.0%). The model performances of the final trained models, R^2_{train} for PLSR and R^2_{OOB} for RF (from out-of-bag samples), generally reached similar levels compared to the cross-validation.

All three NO_3-N metrics could be predicted with a reasonably good cross-validated performance, $R^2_{CrossVal} > 0.5$ with the highest value being $R^2_{CrossVal} = 0.69$ for mean NO_3-N concentrations with RF. Performance was substantially lower for PO_4-P: Models for slope *b* of PO_4-P only reached $R^2_{CrossVal} > 0.4$ and mean concentrations $R^2_{CrossVal} > 0.3$, whereas the models CV_C/CV_Q only reached $R^2_{CrossVal} < 0.3$. For TOC, mean concentrations were well explained with $R^2_{CrossVal} > 0.5$, whereas the *C*-*Q* metrics CV_C/CV_Q and slope *b* only reached $R^2_{CrossVal} < 0.3$. The descriptors with the highest ranks are given in Table 3 (Tables S5–S7 for complete results), however, the interpretation of variable importance is limited for models with low overall explained variability.

For mean NO_3-N concentrations, both PLSR and RF models rank the fractions of forest highest, directly followed by agricultural land cover and top soil C/N ratio in PLSR. In the PLSR model, there is a prominent difference in variable importance to the next descriptors, which are the vertical concentration heterogeneity, fractions of sand and clay (all three with a positive direction of influence) and the fraction of sedimentary aquifer. The RF model marks a step in variable importance after the first rank (f_forest), which is followed by mean annual and seasonality of precipitation, fraction of sedimentary aquifer, vertical heterogeneity and fraction of agriculture on rank 6. For explaining the NO_3-N dynamics (*b* and CV_C/CV_Q), the descriptor vertical heterogeneity has the highest importance (first rank in three of the four models). The PLSR model coefficients indicate a positive link, meaning that the slope *b* tends to be higher in areas with high vertical contrast between potential seepage and groundwater NO_3-N concentrations. Only the RF model for slope *b* of NO_3-N ranks the topographic descriptors (slope_mean, twi_mean, dem_mean) highest, which also appear highly ranked in the other models for NO_3-N export dynamics following het_v. The variables depth to bedrock and fraction of sedimentary aquifer also obtain high importance values.

For mean PO_4-P concentrations, the P load from point sources stands out with the highest variable importance in both models, a large step to the second ranked variables and a positive coefficient in PLSR. Slope *b* of the *C*-*Q* relationship is best explained by mean N surplus and the fraction of sedimentary aquifers, all with a positive relationship. After a step in variable importance, these three variables are followed by the 90th percentile of the TWI, the P content in the topsoil and the frequency, amount and seasonality of precipitation.

Mean TOC concentrations are best explained by the TWI (90th percentile and mean) based on PLSR and by mean elevation and topographic slope based on RF. The other respective topographic variables also turn out highly ranked in the models together with the fraction of sedimentary aquifers, potential evapotranspiration and depth to bedrock. The TOC dynamics of the complete set of study catchments were only poorly explained by the available predictors with a maximum $R^2_{CrossVal} = 0.28$ (RF for slope *b*). However, hydrological parameters (Table S11) substantially increased the variance explained by the PLSR and RF models between 11% and 37% (with $R^2_{CrossVal} = 0.44$ for slope *b* in RF and $R^2_{CrossVal} = 0.58$ for CV_C/CV_Q in PLSR) for the smaller subset of catchments ($n = 184$). Especially the flashiness index, seasonal ratio of discharge and BFI ranked high, with a positive direction of influence.

3.4. Relationships Among the Nutrient Export Metrics

All metrics correlated positively for NO_3-N and PO_4-P. This correlation was strongest for CV_C/CV_Q ($r = 0.55$) and lowest for slope *b* ($r = 0.19$, Figure 4). Over the whole range of catchments, the lowest mean NO_3-N and PO_4-P were linked to the highest f_forest (Figure 5a).

For NO_3-N and TOC, mean TOC correlated positively with the NO_3-N export metrics (CV_C/CV_Q $r = 0.58$ and slope *b* $r = 0.52$); this correlation was also apparent for the respective TOC export metrics but was less pronounced. The mean TOC and the slope of NO_3-N also both correlated to the twi_90p ($r = 0.76$ and 0.53 respectively, Figures 5b and S5). Catchments with a high twi_90p tended to have high mean TOC and low mean NO_3-N concentrations (Figure 5c), whereas high NO_3-N concentrations were mostly observed in catchments with lower twi_90p and lower mean TOC concentrations.

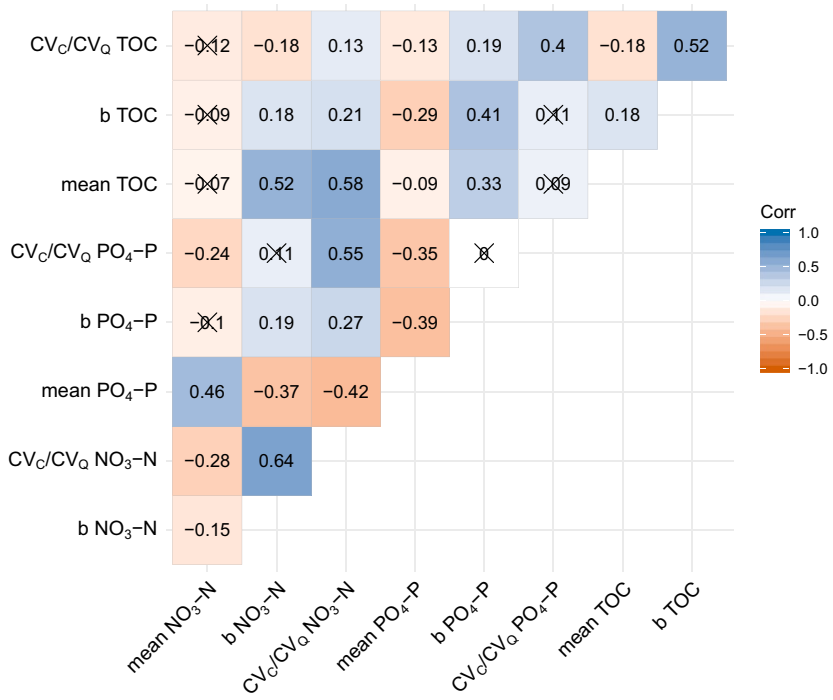

Figure 4. Spearman rank correlation matrix between metrics of the export regimes. Crosses mark non-significant correlations (significance level of 0.05).

For PO_4-P and TOC, slope *b* of PO_4-P correlated positively and mean PO_4-P concentration negatively with all TOC metrics, with the correlation coefficient between the slopes *b* being the highest ($r = 0.41$). *C-Q* slopes *b* of PO_4-P were related to high twi_90p ($r = 0.46$, Figures 5d and S5), which was also a slight tendency for TOC ($r = 0.28$).

4. Discussion

We first discuss the observed export dynamics and their controls for each nutrient individually, followed by a section on nutrient interactions, a synthesis and an implication section.

4.1. Nutrient-Specific Export and Controls

4.1.1. NO_3-N: Natural Attenuation Buffers Input and Controls Export Regimes

The variability in mean NO_3-N concentrations among the studied catchments was linked to the land use, as the fractions of forest and of agriculture both ranked high in the PLSR and RF models and relate to low and high diffuse N sources, respectively. This agrees with findings of previous studies (e.g., Evans et al., 2014; Hansen et al., 2018; Minaudo et al., 2019; Musolff et al., 2015). The fraction of either forest or agriculture alone could respectively explain 32% or 29% of this variability in a simple linear regression case, while in the PLSR and RF the total variability explained by all descriptors was between 64% and 70%. The correlation with N surplus was lower ($r = 0.39$ N_surp_80, Figure S5) even though it is strongly related to agricultural land ($r = 0.71$, Figure S4). This is related to a few catchments that have exceptionally high N surplus but moderate mean NO_3-N concentrations.

However, the relationship between the fraction of agriculture and the mean NO_3-N concentration is highly heteroscedastic as shown in Figure 6a. We found that deviations from a positive linear relationship between the proxies for N input and N output are related to soil and aquifer properties, as e.g. f_sedim ranked high in the PLSR and RF (Tables 3 and S6). This could indicate buffering of inputs by natural attenuation (removal by denitrification) in the unsaturated and saturated zones. Adding the fraction of sedimentary aquifer as a

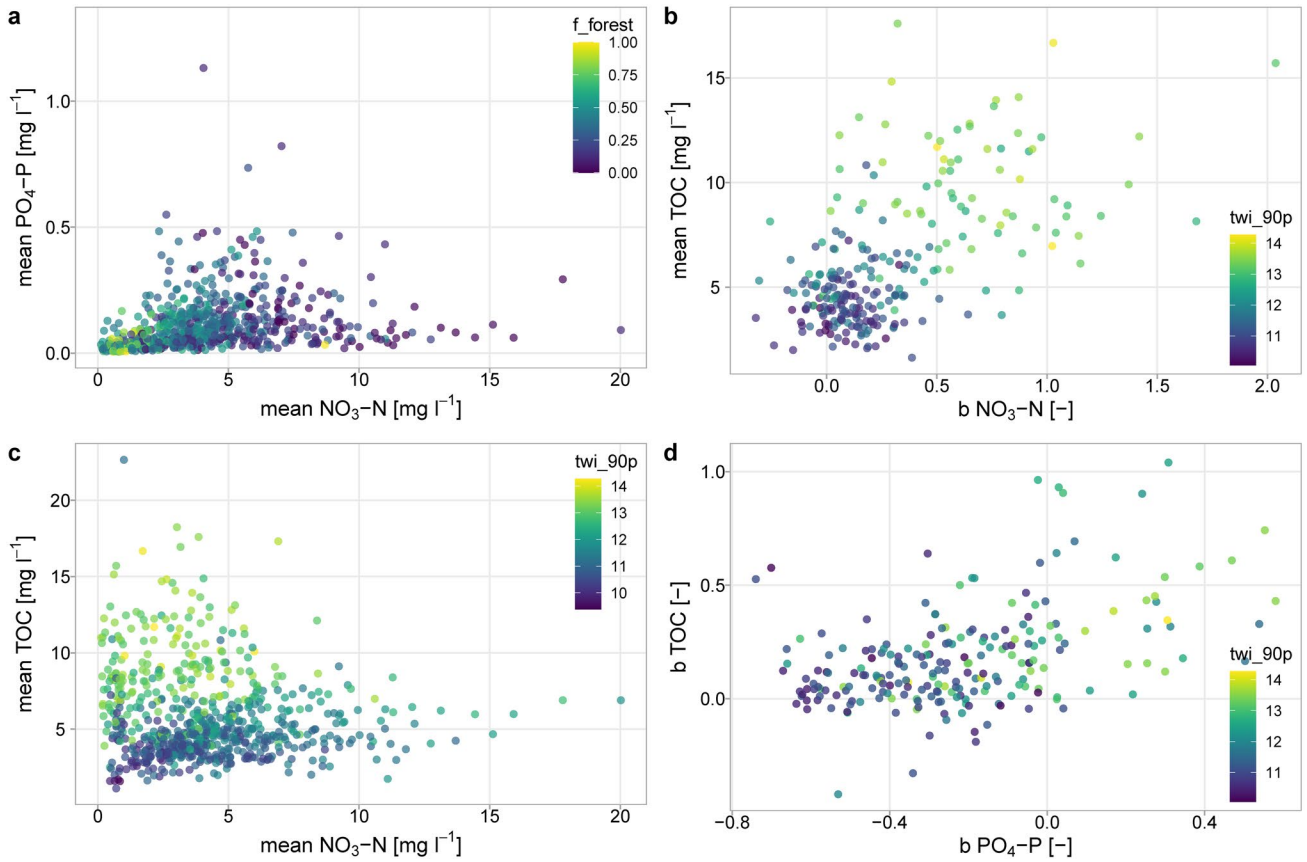

Figure 5. Interaction between metrics of different nutrients: (a) mean PO_4-P against mean NO_3-N concentrations, (b) mean TOC against b NO_3-N, (c) mean TOC against mean NO_3-N concentrations, and (d) slope of PO_4-P against TOC.

secondary factor to the linear model with forest (or agriculture) fractions increased the explained variability by 20%–52% (or 49%) respectively. Previous studies have shown that sedimentary aquifers often exhibit a high denitrification potential (Hannappel et al., 2018; Knoll et al., 2020; Kunkel et al., 2004). Unconsolidated aquifers are usually deep, low-land aquifers linked to long travel times (Merz et al., 2009; Wendland et al., 2008) with anaerobic conditions and organic carbon or pyrite deposits providing electron donors for denitrification, especially in the lowlands of northern Germany (Kunkel et al., 2004; Wendland et al., 2008). Both long residence times and favorable conditions for denitrification increase the potential for NO_3 removal along the flow path (Rivett et al., 2008). This link is supported by het_v (ranked 4th and 5th) representing the vertical NO_3 concentration contrast. This contrast likely results from denitrification under anaerobic subsurface conditions (Knoll et al., 2020) and correlates positively with f_sedim (r = 0.68, Figures S4, and 6d). Denitrification in riparian wetlands, which are more abundant in lowlands, could additionally buffer NO_3-N inputs and create a link to the carbon cycle (see also Section 4.2.) (Pinay et al., 2015; Sabater et al., 2003). Apart from effective N removal by denitrification, the decrease in concentration could also be linked to the large groundwater storages of deep, sedimentary aquifers causing high dilution by old (pre-industrial) water fractions low in NO_3-N concentrations and the resultant contrast in vertical concentrations. In such cases, the system would not be equilibrated in terms of its N balance within the investigated time frame (Ehrhardt et al., 2019). Additionally, in-stream retention could also be higher in areas with low slopes due to longer residence times in the river network.

Godsey et al. (2019) showed a general hydroclimatic modification of average concentrations of geogenic solutes. Here, we find a similar pattern with the annual mean and seasonality of precipitation which ranked high in the RF model. Climatic characteristics like the lowest mean annual precipitation, a relatively high ratio between summer to winter precipitation (P_SIsw), and the highest aridity are found in eastern

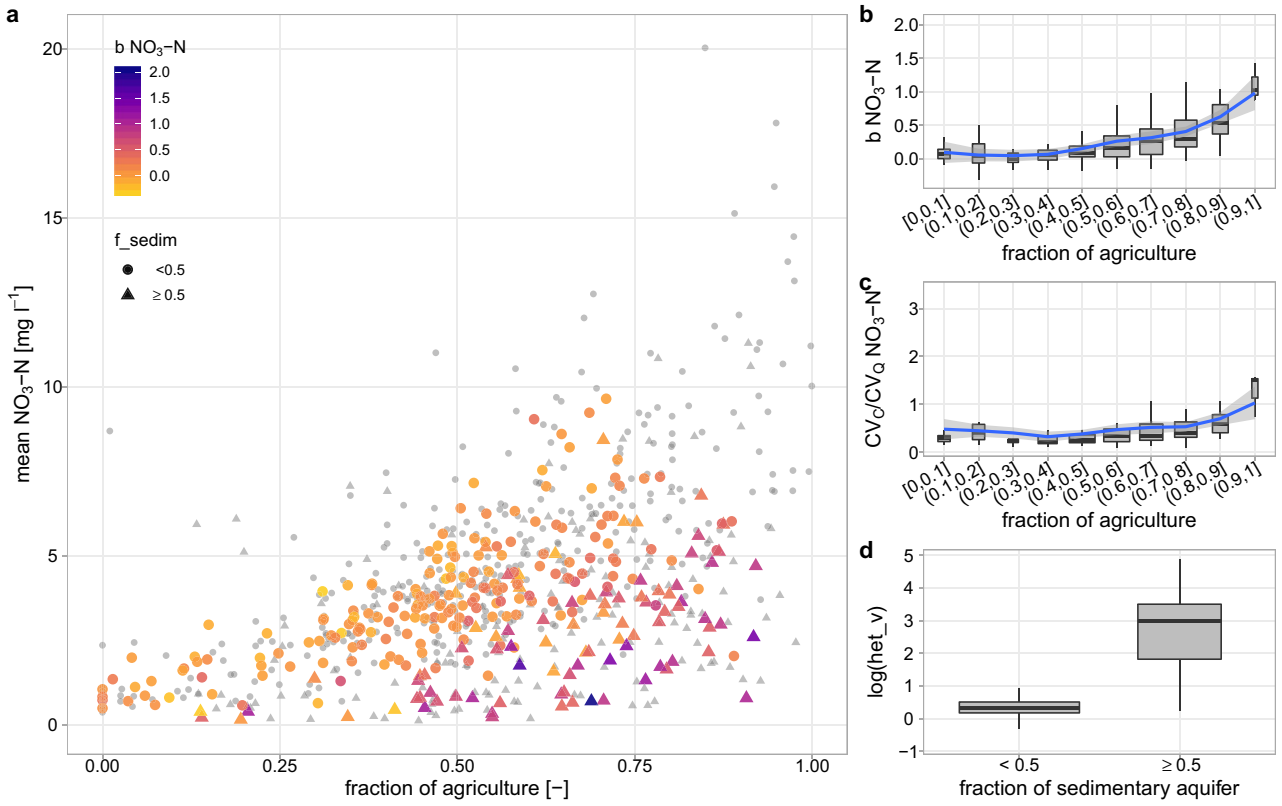

Figure 6. Relationship between the fraction of agriculture as a proxy for diffuse source strength of N and (a) mean NO_3-N concentrations in combination with aquifer type (f_sedim) and NO_3-N export patterns, (b) slope *b* of NO_3-N as binned boxplots, (c) CV_C/CV_Q as binned boxplots, and (d) the link between the fraction of sediments and vertical concentration heterogeneity. In panel (a) the colors indicate the slope *b* of the *C*-*Q* relationship, small gray dots belong to catchments without slope *b* due to missing *Q* data. The shape indicates whether the sedimentary aquifer type dominates. For (b), (c), and (d) the boxplot width is defined by sample size. Blue line with gray shading in (b) and (c) indicate a LOESS regression with confidence interval (confidence level 0.95).

Germany which coincides with highest mean NO_3-N. This suggests an imprint of regional hydro-climate on a lower dilution potential in eastern German catchments.

Altogether, this clearly indicates that the anthropogenic N-input from diffuse sources is a first order control for mean riverine NO_3-N concentrations, while natural attenuation is able to buffer the high inputs (especially in lowlands with deep aquifers), whereas hydroclimatic conditions seem to play a subordinate role.

We found significantly higher mean NO_3-N concentrations for the class of catchments with low concentration variability, that is chemostatic regimes ($CV_C/CV_Q < 0.5$, Figure 2b). This finding agrees with those of Thompson et al. (2011), who found significantly lower CV_C/CV_Q for the group of catchments with higher NO_3-N export and hypothesized that such behavior was due to the homogenization of sources in highly managed catchments. However, in our study, we found that part of the intensively managed catchments exhibited surprisingly low mean NO_3-N concentrations combined with high concentration variability (Figure 6a). For our data set, these agricultural catchments with very high concentration variability led to a tendency of catchments with higher fraction of agriculture linking to higher slope *b* and CV_C/CV_Q (Figures 6b and 6c), although overall chemostatic export prevailed for the majority of the study catchments. More specifically, around 34% of the agriculturally dominated catchments (f_agric ≥ 0.5) exhibited chemodynamic export regimes, out of which 89% were combined with enrichment patterns, compared to 17% of chemodynamic catchments for less agricultural catchments (f_agric < 0.5). Our study therefore does not support the generality of the hypothesis that highly managed, agricultural catchments are necessarily subject to homogenization of sources and thus to chemostatic export regimes (Basu et al., 2010; Thompson et al., 2011). Thus, we recognize that there are agricultural catchments in our study that exhibit chemostatic export, but high fractions of agriculture did not necessarily induce chemostasis and neutral *C*-*Q* patterns. The agricultural chemodynamic catchments widely coincided with catchments where a high abundance of

sedimentary aquifers and strong vertical concentration heterogeneity prevailed, as also evident in PLSR and RF models (Table 3, Figure 6a and 6d).

The variability in the export dynamics, that is regimes (CV_C/CV_Q) and patterns (slope *b*), between the studied catchments was positively linked to the descriptor het_v representing the average vertical NO_3-N heterogeneity from soils to groundwater within each catchment. This means that the larger the concentration gradient is over depth within the catchments subsurface, the more chemodynamic and enriching the NO_3-N export. This concentration gradient can be a result of subsurface reactivity such as denitrification in groundwater. In contrast, the variables of horizontal source heterogeneity het_h and sdist_mean did not explain differences in concentration dynamics among the catchments. Accordingly, our results from this data-driven approach confirm findings from previous modeling studies: Zhi et al. (2019) found vertical concentration gradients in combination with end-member mixing, and Musolff et al. (2017) found the concentration gradient over travel times (a more general, indirect measure of solute source heterogeneity) to control *C*-*Q* patterns. The linkage between vertical concentration heterogeneity and export patterns is plausible considering that agricultural and atmospheric N inputs enter the subsurface from the top. A top-loaded profile in combination with the dominance of young water contribution to discharge from upper soil layers during high flows and the dominance of old water fractions at base flow conditions (exponential saturated hydraulic conductivity profile) causes a positive *C*-*Q* slope. This interpretation coincides with the concept of juxtaposition of discharge generation and concentration profiles by Seibert et al. (2009) and with the scenario of higher concentrations linked to shorter travel times described by Musolff et al. (2017). Additionally, tile drainages can enhance the effect of concentration heterogeneity by increasing the younger water fraction during high-flows and by avoiding potential retention zones (Musolff et al., 2015; Van der Velde et al., 2010; Van Meter & Basu, 2017). As geoinformation on drainages over the large study region is not available, we cannot prove the role of this additional flow path in this study.

We found that both the diffuse input and the reactivity (the combined effect of reaction rates and residence times) resulting in NO_3-N attenuation along the flow paths might determine the strength of vertical concentration heterogeneity. Consequently, chemodynamic export with enrichment patterns could indicate natural attenuation and effective denitrification under high inputs. In turn, chemostasis could be an indication of missing reactivity in the catchment in concert with large legacy N pools (Basu et al., 2010). Chemodynamic export may also occur when vertical concentration contrasts emerge in large groundwater bodies not yet in temporal equilibrium (as stated above). However, concentration gradients will only be maintained over a longer term if subsurface attenuation occurs or input changes. The relationship between input, attenuation and export patterns (Figure 6) also indicates that catchments with relatively low mean NO_3-N concentrations but high inputs and steep positive *C*-*Q* patterns might still be "hot spots" in terms of exported loads, eutrophication risk, and large N legacies. Here, the natural attenuation might buffer inputs in terms of mean riverine and groundwater concentrations but not necessarily the exported loads during high flows when concentrations are considerably higher.

4.1.2. PO_4-P: Unexpected Strong Control of Diffuse Sources on Export Patterns

Mean PO_4-P concentrations were positively linked to direct anthropogenic input from point sources, although the overall explained variance in the PLSR and RF models was surprisingly low ($R^2_{CrossVal} = 0.34$ and 0.40). Previous studies have also demonstrated the strong control of point sources on average riverine total P concentrations (Minaudo et al., 2019; Westphal et al., 2019; Withers & Jarvie, 2008), with their contributions remaining high even after significant reductions of inputs from point sources (Behrendt et al., 1999; Westphal et al., 2019). However, even in a densely populated catchments (about 460 inhabitants km^{-2}), contributions of point sources to total P can be similar to diffuse sources, for example about 60% at load peak and 40% with modern wastewater treatment (Westphal et al., 2019).

In general, PO_4-P is subject to P cycling including retention, transformation and remobilization processes in the stream (Jarvie et al., 2012; Smolders et al., 2017; Withers & Jarvie, 2008), all of which may vary strongly in space and time (Withers & Jarvie, 2008). In-stream retention capacities were estimated to 36% of the P loads (Westphal et al., 2019) and even up to 50% of PO_4-P and 60% of total P in other catchments (Withers & Jarvie, 2008). P cycling thus affects both the timing and the load of exported P and potentially reshapes direct inputs and delivery from land-stream transfer at catchment scale (Casquin et al., 2020; Jarvie et al., 2012). This could explain why mean PO_4-P concentrations are linked to the inputs but are hardly

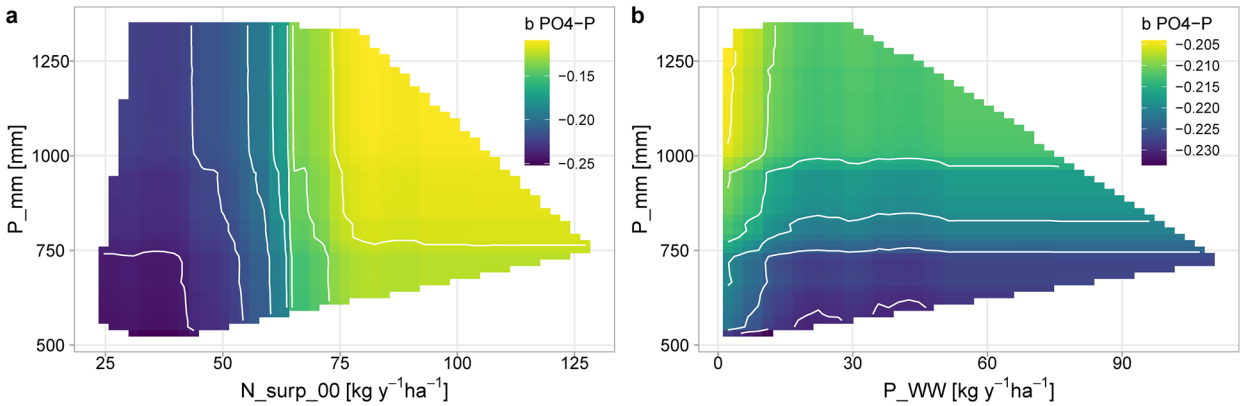

Figure 7. Partial dependence plots for RF model for slope *b* of PO_4-P showing the interaction between (a) N surplus (N_surp_00) and (b) P loads from point sources (P_WW) with mean annual precipitation (P_mm). Colors indicate the range of predicted *b* values with mean values for the other descriptors, which differ for (a) and (b) due to different sensitivities. White areas are outside the covered parameter space (without extrapolation). RF, random forests.

predictable by average catchment characteristics which do not adequately represent controls of in-stream processes. Other reasons for the low predictability could be uncertainties related to (1) the point source data which do not account for potential temporal variations in the loading and small rural point sources (e.g., from farmyards or septic tanks, Withers & Jarvie, 2008), or (2) the sampling frequency of *C* which potentially misses moments of peak concentrations and leads to an underestimation of mean PO_4-P, as shown by Hunsaker and Johnson (2017).

For PO_4-P export dynamics, dilution patterns prevailed in two thirds of the catchments, a finding which agrees with previous studies on association with point-source dilution (Bowes et al., 2015; Moatar et al., 2017) or biogeochemical processes releasing PO_4-P during summer low-flows and thus mimicking point sources in riparian zones (Dupas et al., 2018) and riverbed sediments (Smolders et al., 2017). In 11% of the catchments, we found enrichment patterns of PO_4-P which have also been observed in other cases, for example through mobilization of diffuse sources from agricultural areas (Bieroza & Heathwaite, 2015; Rose et al., 2018) and from a nutrient-rich O-horizon in a forested catchment (Hunsaker & Johnson, 2017) during storm events.

N surplus and the fraction of sedimentary aquifers turned out to be the dominant predictive variables for slope *b* of PO_4-*Q* relationships and were positively linked to it, even with prevailing dilution patterns (Figure 7a, Table 3). Both variables together explain 42% of the variability in slope *b*, and individually 27% and 26% respectively based on a linear model. This constitutes a large part of the explained variability of all descriptors (R^2_{CrossVal} spans 0.43–0.47). Especially in northwestern and southeastern Germany, catchments with high N surplus tended to show enrichment patterns for PO_4-P (Figure 3). High P applications (especially from manure) and low P use efficiencies led to widespread P accumulation (legacy) on agricultural soils, increasing the risk of P losses (Osterholz et al., 2020; Schoumans et al., 2015; Sharpley et al., 2013). Areas with prevailing enrichment patterns coincide with regions of intense manure applications from livestock farms (Häußermann et al., 2019) and high degrees of P saturation (Fischer et al., 2017), which could be the reason for the enhanced PO_4-P land-to-stream transfer. This is reflected in the PLSR model as the topsoil P content (soil_P) positively linked to slope *b* and ranks order 5. Furthermore, Fischer et al. (2017) found widespread (>76%) high risks of dissolved P loss from German agricultural soils, so that the process of diffuse P mobilization is likely to occur in more than 11% of the catchments but might be less pronounced in catchments where dilution prevails. P saturation in the topsoil can be considered as source heterogeneity with a top-loaded profile. The high ranks of f_sedim and twi_90p in the PLSR, explaining slope *b* of PO_4-P, could indicate the additional influence of tile drains in wet lowland soils. Tile drains and preferential flow paths were shown to enhance the land-to-stream transfer of P and cause positive *C*-*Q* patterns by increasing the connectivity of soil P sources and bypassing of potential sinks in the soil matrix (Gentry et al., 2007; Osterholz et al., 2020).

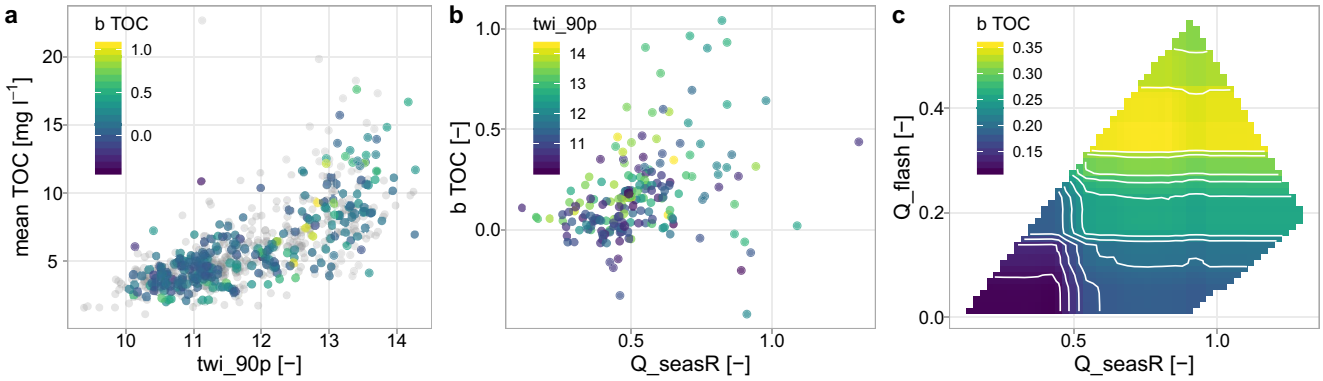

Figure 8. Observed mean TOC concentrations against twi_90p with colors according to slope *b* of TOC (a), observed slope b of TOC against seasonality of discharge (Q_seasR, see Table S2) with colors representing the twi_90p (b), and partial dependence plot of slope *b* TOC from RF model for the variables seasonality and flashiness of discharge (Q_seasR, Q_flash) (c). Note that gray dots in (a) belong to catchments without *Q* data. RF, random forests.

Climatic controls were also ranked high in the PLSR and RF models, for example mean annual precipitation (P_mm) showed a positive impact on slope *b* of PO_4-P (Figure 7, Table 3). The PLSR and RF models including additional hydrological descriptors indicate that a lower seasonal *Q* ratio (i.e. low summer *Q* compared to winter) relate to lower slope *b* and takes over the rank of P_mm in these models (Table S7). This suggests that the impact of P_mm relates to a stronger dilution of low-flow concentrations during the summer and thus less pronounced PO_4-P dilution export patterns.

Although point sources (P_WW) were not part of the highly ranked predictors, the correlations of slope *b* with mean PO_4-P concentrations ($r = -0.39$, see Figure 5), together with the fact that point sources also partly explain mean PO_4-P concentrations, suggest some influence of point sources on slope *b*. This is reflected in the partial dependence plots showing the higher impact of N surplus on slope *b* compared to point sources and climatic drivers (Figure 7). The impact of point sources is only visible for low P loads (<15 kg ha^{-1} y^{-1}), suggesting possible threshold behavior. The lack of an expected clear relationship between point sources and slope *b* fits to the above interpretation that in-stream P cycling can significantly reshape P concentration dynamics (Casquin et al., 2020; Jarvie et al., 2012). The still prevailing dilution patterns of PO_4-P could thus be related to biogeochemically induced P release (see above, Dupas et al., 2018; Smolders et al., 2017) besides the climatic controls.

4.1.3. TOC: Flat Topography Strengthens Sources and Hydrology-Driven Export

Topography related characteristics appeared to dominantly control mean TOC, for example twi_90p and twi_mean alone already explain 52% of the variability in a linear model (Figure 8a). This topography control agrees with previous results by Zarnetske et al. (2018), who found the topographic slope and the share of wetlands followed by mean annual precipitation to best predict DOC concentration levels across the contiguous USA. Musolff et al. (2018) also reported the twi_90p as a good predictor for median DOC concentrations in small mountainous, mainly forested German catchments. The twi_90p can also be interpreted as a proxy for the extent of riparian, well-connected wetlands (Musolff et al., 2018), source areas of organic matter and thus TOC (Bishop et al., 2004; Laudon et al., 2004). Mean TOC concentrations across the studied catchments were not connected to wastewater point sources, suggesting that on a larger spatial extent, terrestrial sources overwhelm potential point source inputs. This is in line with findings of Gücker et al. (2006) on TOC inputs from modern wastewater treatment plants, indicating no consistent effect on downstream TOC concentrations.

Most catchments across Germany classified as enrichment patterns and chemostatic regimes for TOC, which align along the findings of previous studies on dominance of enrichment patterns and transport-limited export for DOC and TOC (Moatar et al., 2017; Musolff et al., 2018; Zarnetske et al., 2018). Zarnetske et al. (2018) found hydrologically well-connected wetlands to control these patterns, while Musolff et al. (2018) found high twi_90p, soluble reactive phosphorus, pH and aridity index to relate to high DOC variability. The near stream, well-connected wetlands can be interpreted as horizontal source heterogeneity

and could cause the observed enrichment patterns. However, the fraction of wetland, the twi_90p and the climatic characteristics, together with the other characteristics used, could not satisfactorily explain the variability in the export metrics observed across German catchments. In Moatar et al. (2017), DOC-*Q* slopes correlated with various hydrological variables and, in Musolff et al. (2015), the variability in TOC dynamics were well explained by the BFI (+), artificial drainages (−) and topographic slope (+). In agreement, the subset analysis with hydrological descriptors (Table S11) showed that catchments with more equilibrated discharge patterns (i.e., less flashy, similar summer and winter *Q* with Q_seasR close to 1, and higher base flow) tend to mobilize TOC more dynamically with *Q* but also show a higher variability in the export patterns (Figures 8b and 8c). Antecedent conditions (especially riparian soil temperatures and moisture) are known to control DOC production and therefore could shape the export patterns in combination with temporally variable hydrological connectivity (Wen et al., 2020; Winterdahl et al., 2011). Variable antecedent conditions can cause variable source heterogeneity, resulting in export variability in time and space. The identified hydrological controls (flashiness, seasonality, and BFI) quantify the temporal variability of hydrological conditions and thus might implicitly represent the variability of antecedent conditions within a catchment.

However, even with hydrological descriptors, part of the variability in TOC export dynamics between the studied catchments remains unexplained. This may be linked to other drivers of TOC export besides *Q*, such as the temperature (Musolff et al., 2018; Winterdahl et al., 2014). However, the influence of mean air temperature on the *C*-*Q* relationships cannot be found in our study catchments. We observed that discharge strongly controls the TOC concentrations (high R^2 in the *C*-*Q* relationships) only in study catchments with flatter topography: for TOC-*Q* relationships with $R^2 \geq 0.5$, the topographic slope was <2.1° and twi_90p > 12.2, whereas the catchments with lower R^2 had a higher mean topographic slope = 4.3° and lower mean twi_90p = 11.7.

4.2. N-P-OC: Do Riparian Wetlands Control Observed Nutrient Interactions?

Riparian wetlands are potential hot spots of biogeochemical processes due to high hydrologic connectivity to the streams and variable redox conditions during dry and wet cycles with changing water tables (Burt, 2005; McClain et al., 2003). The twi_90p, a proxy for the extent of riparian wetlands (Musolff et al., 2018), was found to be an important predictor for several of the export metrics (mean TOC concentrations and slope *b* of NO_3-N and PO_4-P) and could be linked to some covariance (Figure 5).

Mean NO_3-N and PO_4-P showed a positive, heteroscedastic relationship with the lowest values of both nutrients in the most forested, pristine catchments (Figure 5a). A negative relationship would be expected in catchments with high twi_90p if reductive mobilization prevailed (Dupas, Gruau, et al., 2015; Gu et al., 2017), however, even catchments without point source influence exhibited a positive relationship. We argue that the anthropogenic impact (in terms of N and P inputs) dominates in the studied catchments and that potential biogeochemical interactions between NO_3-N and PO_4-P do not control the spatial variability of mean concentrations among catchments.

The catchments with the highest twi_90p mostly exhibited relatively high mean TOC and low mean NO_3-N concentrations (Figure 5c). This relationship could be linked to denitrification under anoxic conditions, that is, the redox reaction with DOC as the electron donor and NO_3 as acceptor, as has been observed and discussed in several previous studies (e.g., Cabezas et al., 2013; Taylor & Townsend, 2010). Thus, riparian wetland denitrification could be part of the high natural NO_3-N attenuation in lowlands (see Section 4.1.1.) and intensify positive NO_3-*Q* relationships due to reduced summer low-flow concentrations. However, as the twi_90p is also correlated to het_v ($r = 0.75$), which was the dominant control of slope *b* of NO_3-N, the additional contribution of this interaction within riparian wetland cannot be fully disentangled here.

The positive link between slope *b* of PO4-P and TOC with the twi_90p (Figure 5d) suggests that both nutrients could be mobilized in riparian wetlands, however with a high variability. The mobilization could be linked to iron dissolution under reducing conditions, e.g. due to decreasing NO_3 concentrations as redox buffers, as discussed for example by Cabezas et al. (2013).

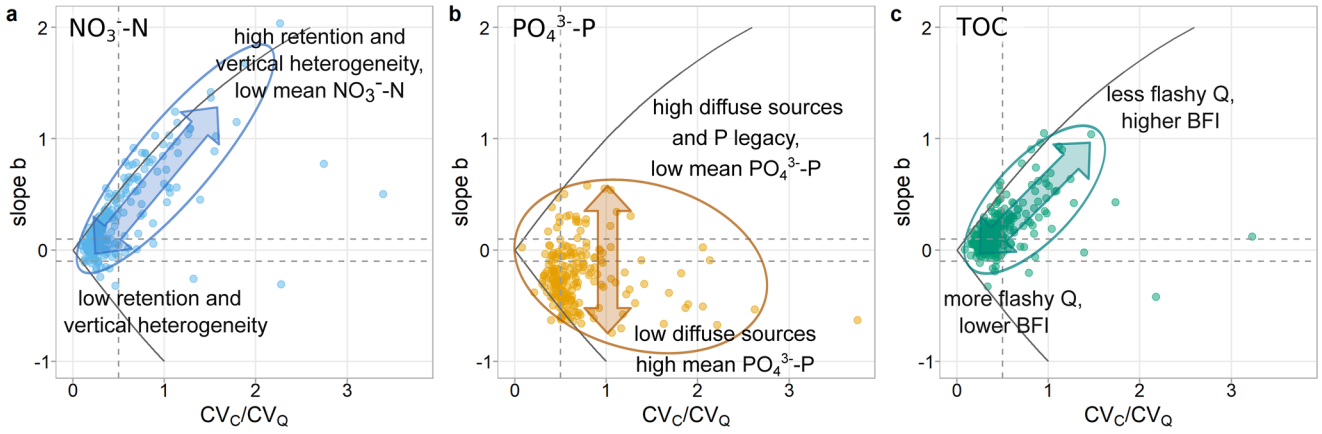

Figure 9. Archetypal ranges of solute-specific export patterns and regimes with arrows along the main axis of variability explained by the identified dominant characteristics (labels at the end) for (a) NO_3-N, (b) PO_4-P, and (c) TOC. The ellipses surround the archetypal ranges including most of the catchments. BFI, base-flow index.

4.3. Archetypal Ranges of Nutrient Export

Over the wide range of investigated catchments, we found solute-specific ranges of export metrics (Figures 2 and 9). The classification of the export dynamics revealed that about 70% of the catchments group into the respective dominant class for each nutrient. This solute-specific prevalence of one pattern or regime has also been reported previously, for example by Minaudo et al. (2019), Moatar et al. (2017) and Zarnetske et al. (2018). The consistency of export type of a specific nutrient might be surprising, considering the multitude of processes affecting nutrient cycling, mobilization, transport, and retention. The properties such as the solubility of each constituent have a major control over processes that lead to mobilization, transport and reactivity, and thus define the archetypal range of export dynamics. The variability within these ranges can be partly linked to catchment characteristics such as the source strength and its spatial arrangement as shown and addressed by PLSR and RF (see Section 3.3).

The dominant controls of the spatial variability of export dynamics and prevailing characteristics for specific areas within the solute-specific ranges (discussed in the preceding sections) are synthesized in Figure 9. For NO_3-N, we found a strong interaction between anthropogenic and natural controls: while agricultural inputs define a baseline for mean NO_3-N concentrations, natural attenuation creates deviations lowering the mean NO_3-N. This attenuation likely increases vertical concentration heterogeneity, and is thus reflected in chemodynamic enrichment patterns. For PO_4-P, anthropogenic footprints from point sources (shaping mean PO_4-P) and diffuse sources (shaping positive *C*-*Q* slopes) seem to interact with more natural controls of P cycling, reshaping the in-stream concentration dynamics and creating a wide range of variability. For TOC, interaction between anthropogenic and natural controls was not apparent, as the topography strongly controlled mean TOC and as the spatial variability of export dynamics was partly explained by hydrological variability.

In summary, we found the hypothesis that diffuse source heterogeneity widely controls export dynamics to be partially confirmed for analyzed nutrients in the study catchments. For NO_3-N, export dynamics were widely controlled by vertical concentration heterogeneity which might be a result of subsurface reactivity as the dominant process (Section 4.1.1). Strong enrichment patterns occurred in areas with high concentration heterogeneity, whereas, chemostatic export prevailed with concentration homogeneity. For PO_4-P, the strength of diffuse sources was dominant, suggesting that heterogeneity in P soil status between top soil and deeper subsurface layers drives export patterns. The generally positive TOC-*Q* relationships could be linked to heterogeneously distributed, near stream sources, however, the extent of riparian wetlands could not explain the variability among the catchments. The hydrology might control variations in source strength and heterogeneity causing temporal variability in the *C*-*Q* relationships. For both PO_4-P and TOC, directly hydrologically connected areas are prerequisite for translating vertical source heterogeneity to chemodynamic

export due to their strong sorption tendency. This connectivity can be more pronounced in drained, lowland areas (preferential flow paths) or in locations close to the stream such as riparian zones.

4.4. Implications

Our countrywide analysis of nutrient export dynamics revealed regions of dominant chemostatic and chemodynamic export regimes within Germany (Figure 3), which were partly explained by regionally varying catchment characteristics. Our findings can thus provide orientation for water quality managers about what range of nutrient responses can be expected under specific settings. It could also support decision making for targeted monitoring programmes, as more dynamic systems require higher measurement frequencies to capture their *C*-*Q* variability (Moatar et al., 2020). Observed catchment responses can be used to adapt a targeted management: if chemostatic NO_3-N export is observed, low subsurface denitrification capacity might be the reason and, in consequence, efforts to reduce inputs might be crucial to protect the water quality. In a catchment with apparent effective attenuation and chemodynamic NO_3-N export, the exported loads might still be high and the retention capacity by denitrification might decrease over time, possibly leading to an increase in concentrations in the future. If a system was temporally not in equilibrium (input/output balance), it might exhibit long recovery times. Controlling the inputs thus seems vital in all cases. We found that diffuse sources of PO_4-P can play a large role for P export in German agricultural settings, which demonstrates the need to focus on them in P management besides point sources. The diffuse source mobilization could result in high exported loads, affecting downstream water bodies. Water quality modelers can benefit from the identified dominant controls informing the models to better represent the large-scale observed patterns of different *C*-*Q* dynamics.

As some of the identified controls (especially the anthropogenic ones) have developed over time, the catchment responses may also follow long term trajectories of water quality. For PO_4-P, reductions in point sources and increasing P legacies in agricultural soils might have led to the visibility of enrichment patterns by shifting the dominance of processes. NO_3-N could follow trajectories from more chemodynamic to more chemostatic export if subsurface reactivity decreased over time (Wilde et al., 2017). With rising temperatures and heavier storm events due to climate change (EEA, 2019), biogeochemical interactions linked to temperatures and redox conditions might change. For example, TOC exports might increase with prolonged production times and more variable hydrological connectivity, potentially also enhanced by lower NO_3 redox buffers when depositions and concentrations decrease (Clark et al., 2010).

To further elucidate drivers of nutrient concentrations (including the unexplained variability at catchment scale), the newly assembled data base can be yet explored in terms of nutrient interactions and temporal patterns and their controls. To advance the understanding of the generality of our findings, investigations could be pushed to an even larger, cross-continental scale by adding other national data bases—allowing for greater diversity in hydro-climatic conditions. To complement this national-scale study, studies of selected mesoscale catchments from regions with different observed archetypes using high-frequency data or modeling strategies could further test our derived hypothesis and clarify more of the unexplained variability (Kirchner et al., 2004). Experiments are needed to better characterize and quantify regional denitrification patterns, for example by isotope or trace gas methods.

5. Conclusions

To infer drivers of nutrient export over a wide range of catchments, we analyzed surface water quality and quantity data from a newly assembled, Germany-wide data base. We linked metrics of NO_3-N, PO_4-P, and TOC concentrations and *C*-*Q* relationships of 787 independent catchments to catchment characteristics using multivariate statistical methods. We found that enrichment patterns and chemostatic regimes prevailed for NO_3-N and TOC export, whereas dilution and chemodynamic export prevailed for PO_4-P.

For NO_3-N, we found that subsurface natural attenuation likely buffers anthropogenic diffuse inputs in some catchments reducing mean NO_3-N concentrations and causes vertical concentration heterogeneity

which controls export dynamics. This heterogeneity was largest in lowland areas with deep sedimentary aquifers. Accordingly, enrichment patterns in agricultural areas could indicate effective subsurface reactivity.

Anthropogenic diffuse and point sources were found relevant for PO_4-P concentrations even if the spatial variability in responses was hardly predictable by catchment characteristics. Mean PO_4-P were only weakly linked to point sources, while the variability in PO_4-P dynamics was better explained by diffuse agricultural sources and associated P saturation in the top soils. Probably, natural P cycling significantly reshapes in-stream PO_4-P concentrations, which decouples them from the catchments' source configuration and land-stream transfer processes and thus hampers predictions at catchment scale.

Natural topographic settings dominantly controlled TOC concentrations: mean TOC were strongly linked to the abundance of riparian wetlands as source areas. Hydrological descriptors (especially relatively higher summer low-flow discharges and lower flashiness) increased the explained variability of export metrics; however the unexplained part remained high.

Our main hypothesis that diffuse source heterogeneity controls the spatial variability of export patterns was supported for NO_3-N in terms of concentration heterogeneity over depth and for PO_4-P in terms of topsoil P saturation as a top-loaded profile. For TOC, the hypothesis is only indirectly confirmed by the prevalence of enrichment patterns possibly evolving from near stream and thus heterogeneously distributed source areas.

Altogether, we found that NO_3-N and PO_4-P concentrations and dynamics are dominated by anthropogenic inputs, but natural controls significantly buffer or reshape the responses observed at the catchment outlet. For TOC, natural controls dominated.

Our results improve the understanding of controls of nutrient export dynamics and their regional differences. Thus, they can support water quality modeling and management. Further research on large scale subsurface reactivity to test our hypothesis and on temporal changes in export dynamics would deepen our understanding of dominant processes at catchment scale.

Conflict of Interest

The authors declare no conflict of interest.

Acknowledgments
The authors thank the federal authorities for providing water sample data and all contributors to setting up the used data base, including T. Grau, T. Nitz, and J. Dehaspe. The authors thank four anonymous reviewers and the editor for their valuable comments. The authors appreciate Martin Bach and Uwe Häußermann for providing the N surplus data and Soohyun Yang and Olaf Büttner for providing the data of small water treatment plants in Germany. The authors acknowledge the E-OBS data set from the EU-FP6 project UERRA (http://www.uerra.eu) and the Copernicus Climate Change Service, and the data providers in the ECA&D project (https://eca.knmi.nl). The authors further acknowledge several organizations for providing data products used in this study, including the BfG, BGR, SGD, EEA, FAO, IIASA, ISRIC, ISSCAS, and JRC. The authors also greatly appreciate the funding by the Initiative and Networking Fund of the Helmholtz Association through the project Advanced Earth System Modeling Capacity (ESM) (www.esm-project.net). Open access funding enabled and organized by Projekt DEAL.

Data Availability Statement

Datasets for this research are available under Ebeling (2021b), Ebeling (2021a), Musolff et al. (2020) [original data in institutional repository] and Musolff (2020). Further original datasets used for this research are referenced in Table 1 and in the text.

References

Abbott, B. W., Gruau, G., Zarnetske, J. P., Moatar, F., Barbe, L., Thomas, Z., et al. (2018). Unexpected spatial stability of water chemistry in headwater stream networks. *Ecology Letters*, *21*(2), 296–308. https://doi.org/10.1111/ele.12897

Akaike, H. (1974). A new look at the statistical model identification. *IEEE Transactions on Automatic Control*, *19*(6), 716–723. https://doi.org/10.1109/tac.1974.1100705

Ameli, A. A., Beven, K., Erlandsson, M., Creed, I. F., McDonnell, J. J., & Bishop, K. (2017). Primary weathering rates, water transit times, and concentration-discharge relations: A theoretical analysis for the critical zone. *Water Resources Research*, *53*(1), 942–960. https://doi.org/10.1002/2016wr019448

Bach, M., Klement, L., & Häußermann, U. (2016). *Bewertung von Maßnahmen zur Verminderung von Nitrateinträgen in die Gewässer auf Basis regionalisierter Stickstoff Überschüsse. Teil I: Beitrag zur Entwicklung einer ressortübergreifenden Stickstoffstrategie Zwischenbericht*. UBA-Texte, 55/2016. Retrieved from http://www.umweltbundesamt.de/publikationen/bewertung-von-massnahmen-zur-verminderung-von

Ballabio, C., Lugato, E., Fernández-Ugalde, O., Orgiazzi, A., Jones, A., Borrelli, P., et al. (2019). Mapping LUCAS topsoil chemical properties at European scale using Gaussian process regression. *Geoderma*, *355*, 113912. https://doi.org/10.1016/j.geoderma.2019.113912

Basu, N. B., Destouni, G., Jawitz, J. W., Thompson, S. E., Loukinova, N. V., Darracq, A., et al. (2010). Nutrient loads exported from managed catchments reveal emergent biogeochemical stationarity. *Geophysical Research Letters*, *37*(23). https://doi.org/10.1029/2010gl045168

Basu, N. B., Thompson, S. E., & Rao, P. S. C. (2011). Hydrologic and biogeochemical functioning of intensively managed catchments: A synthesis of top-down analyses. *Water Resources Research*, *47*. https://doi.org/10.1029/2011wr010800

Battin, T. J., Kaplan, L. A., Findlay, S., Hopkinson, C. S., Marti, E., Packman, A. I., et al. (2008). Biophysical controls on organic carbon fluxes in fluvial networks. *Nature Geoscience*, *1*(2), 95–100. https://doi.org/10.1038/ngeo101

Behrendt, H., Huber, P., Opitz, D., Schmoll, O., Scholz, G., & Uebe, R. (1999). *Nutrient emissions into river basins of Germany*. UBA-Texte, 75/99. Retrieved from https://www.umweltbundesamt.de/en/publikationen/naehrstoffbilanzierung-flussgebiete-deutschlands

Beven, K. J., & Kirkby, M. J. (1979). A physically based, variable contributing area model of basin hydrology/Un modèle à base physique de zone d'appel variable de l'hydrologie du bassin versant. *Hydrological Sciences Bulletin*, *24*(1), 43–69. https://doi.org/10.1080/02626667909491834

BGBI.1. (1980). *Verordnung über Höchstmengen für Phosphate in Wasch-und Reinigungsmitteln vom 4.6.1980*. PHöchstMengV.

BGR. (2003). Mean annual rate of percolation from the soil in Germany (SWR1000), hydrogeologischer atlas von Deutschland. Retrieved from https://www.bgr.bund.de/DE/Themen/Boden/Bilder/Bod_Themenkarten_HAD_4-5_g.html

BGR. (2018). Bodenübersichtskarte der Bundesrepublik Deutschland 1:250.000 (BUEK250). Soil map of Germany 1:250,000. Retrieved from https://produktcenter.bgr.de/terraCatalog/Start.do

BGR & SGD. (2015). Hydrogeologische Raumgliederung von Deutschland (HYRAUM). Retrieved from https://www.bgr.bund.de/DE/Themen/Wasser/Projekte/abgeschlossen/Beratung/Hyraum/hyraum_projektbeschr.html?nn=1557832

BGR & UNESCO. (2014). International hydrogeological map of Europe 1: 1,500,000 (IHME1500). Digital map data v1.1. Retrieved from http://www.bgr.bund.de/ihme1500/

Bieroza, M. Z., & Heathwaite, A. L. (2015). Seasonal variation in phosphorus concentration-discharge hysteresis inferred from high-frequency in situ monitoring. *Journal of Hydrology*, *524*, 333–347. https://doi.org/10.1016/j.jhydrol.2015.02.036

Bishop, K., Seibert, J., Köhler, S., & Laudon, H. (2004). Resolving the Double Paradox of rapidly mobilized old water with highly variable responses in runoff chemistry. *Hydrological Processes*, *18*(1), 185–189. https://doi.org/10.1002/hyp.5209

BMU. (2000). *Hydrologischer atlas von Deutschland* (N. u. R. Bundesministerium Für Umwelt Ed.). Bonn/Berlin: Datenquelle: Hydrologischer Atlas von Deutschland/BfG.

Bol, R., Gruau, G., Mellander, P.-E., Dupas, R., Bechmann, M., Skarbøvik, E., et al. (2018). Challenges of reducing phosphorus based water eutrophication in the agricultural landscapes of northwest Europe. *Frontiers in Marine Science*, *5*(276). https://doi.org/10.3389/fmars.2018.00276

Botter, G., Basso, S., Rodriguez-Iturbe, I., & Rinaldo, A. (2013). Resilience of river flow regimes. *Proceedings of the National Academy of Sciences*, *110*(32), 12925–12930. https://doi.org/10.1073/pnas.1311920110

Botter, M., Li, L., Hartmann, J., Burlando, P., & Fatichi, S. (2020). Depth of solute generation is a dominant control on concentration-discharge relations. *Water Resources Research*, *56*(8), e2019WR026695. https://doi.org/10.1029/2019wr026695

Bouraoui, F., & Grizzetti, B. (2011). Long term change of nutrient concentrations of rivers discharging in European seas. *The Science of the Total Environment*, *409*(23), 4899–4916. https://doi.org/10.1016/j.scitotenv.2011.08.015

Bouwman, A. F., Bierkens, M. F. P., Griffioen, J., Hefting, M. M., Middelburg, J. J., Middelkoop, H., & Slomp, C. P. (2013). Nutrient dynamics, transfer and retention along the aquatic continuum from land to ocean: Towards integration of ecological and biogeochemical models. *Biogeosciences*, *10*(1), 1–22. https://doi.org/10.5194/bg-10-1-2013

Bowes, M. J., Jarvie, H. P., Halliday, S. J., Skeffington, R. A., Wade, A. J., Loewenthal, M., et al. (2015). Characterising phosphorus and nitrate inputs to a rural river using high-frequency concentration-flow relationships. *The Science of the Total Environment*, *511*, 608–620. https://doi.org/10.1016/j.scitotenv.2014.12.086

Breiman, L. (2001). Random Forests. *Machine Learning*, *45*(1), 5–32. https://doi.org/10.1023/a:1010933404324

Bricker, S. B., Clement, C. G., Pirhalla, D. E., Orlando, S. P., & Farrow, D. R. G. (1999). *National estuarine eutrophication assessment: Effects of nutrient enrichment in the nation's estuaries*. NOAA National Ocean Service Special Projects Office and the National Centers for Coastal Ocean Science. Retrieved from https://ian.umces.edu/neea/pdfs/eutro_report.pdf

Burns, D. A., Pellerin, B. A., Miller, M. P., Capel, P. D., Tesoriero, A. J., & Duncan, J. M. (2019). Monitoring the riverine pulse: Applying high-frequency nitrate data to advance integrative understanding of biogeochemical and hydrological processes. *WIREs Water*, *6*(4), e1348. https://doi.org/10.1002/wat2.1348

Burt, T. P. (2005). A third paradox in catchment hydrology and biogeochemistry: Decoupling in the riparian zone. *Hydrological Processes*, *19*(10), 2087–2089. https://doi.org/10.1002/hyp.5904

Büttner, O. (2020a). *DE-WWTP—data collection of wastewater treatment plants of Germany (status 2015, metadata)*. HydroShare. Retrieved from https://doi.org/10.4211/hs.712c1df62aca4ef29688242eeab7940c

Büttner, O. (2020b). *The waste water treatment data collection for Germany 2015 (DE-WWTP)*. UFZ. Retrieved from https://www.ufz.de/record/dmp/archive/7800

Cabezas, A., Gelbrecht, J., & Zak, D. (2013). The effect of rewetting drained fens with nitrate-polluted water on dissolved organic carbon and phosphorus release. *Ecological Engineering*, *53*, 79–88. https://doi.org/10.1016/j.ecoleng.2012.12.016

Casquin, A., Gu, S., Dupas, R., Petitjean, P., Gruau, G., & Durand, P. (2020). River network alteration of C-N-P dynamics in a mesoscale agricultural catchment. *The Science of the Total Environment*, *749*, 141551. https://doi.org/10.1016/j.scitotenv.2020.141551

Center for International Earth Science Information Network - CIESIN - Columbia University. (2017). *Gridded population of the world, version 4 (GPWv4): Population density, Revision 10*. NASA Socioeconomic Data and Applications Center. Retrieved from https://doi.org/10.7927/H4DZ068D

Clark, J. M., Bottrell, S. H., Evans, C. D., Monteith, D. T., Bartlett, R., Rose, R., et al. (2010). The importance of the relationship between scale and process in understanding long-term DOC dynamics. *The Science of the Total Environment*, *408*(13), 2768–2775. https://doi.org/10.1016/j.scitotenv.2010.02.046

Conley, D. J., Paerl, H. W., Howarth, R. W., Boesch, D. F., Seitzinger, S. P., Havens, K. E., et al. (2009). ECOLOGY: Controlling eutrophication: Nitrogen and phosphorus. *Science*, *323*(5917), 1014–1015. https://doi.org/10.1126/science.1167755

Copeland, C. (2016). *Clean water act: A summary of the law* [press release]. Congressional Research Service. Retrieved from https://fas.org/sgp/crs/misc/RL30030.pdf

Cornes, R. C., van der Schrier, G., van den Besselaar, E. J. M., & Jones, P. D. (2018). An ensemble version of the E-OBS temperature and precipitation data sets. *Journal of Geophysical Research: Atmospheres*, *123*(17), 9391–9409. https://doi.org/10.1029/2017jd028200

Damania, R., Desbureaux, S., Rodella, A.-S., Russ, J. D., & Zaveri, E. D. (2019). Quality unknown : The invisible water crisis (Report No 140973). World Bank. Retrieved from https://openknowledge.worldbank.org/handle/10986/32245

De Jager, A., & Vogt, J. (2007). *Rivers and catchments of Europe—catchment characterisation model (CCM)*. Joint Research Centre. Retrieved from http://data.europa.eu/89h/fe1878e8-7541-4c66-8453-afdae7469221

Diamond, J. S., & Cohen, M. J. (2018). Complex patterns of catchment solute-discharge relationships for coastal plain rivers. *Hydrological Processes*, *32*(3), 388–401. https://doi.org/10.1002/hyp.11424

Dupas, R., Delmas, M., Dorioz, J.-M., Garnier, J., Moatar, F., & Gascuel-Odoux, C. (2015). Assessing the impact of agricultural pressures on N and P loads and eutrophication risk. *Ecological Indicators*, *48*, 396–407. https://doi.org/10.1016/j.ecolind.2014.08.007

Dupas, R., Gruau, G., Gu, S., Humbert, G., Jaffrézic, A., & Gascuel-Odoux, C. (2015). Groundwater control of biogeochemical processes causing phosphorus release from riparian wetlands. *Water Research*, *84*, 307–314. https://doi.org/10.1016/j.watres.2015.07.048

Dupas, R., Jomaa, S., Musolff, A., Borchardt, D., & Rode, M. (2016). Disentangling the influence of hydroclimatic patterns and agricultural management on river nitrate dynamics from sub-hourly to decadal time scales. *The Science of the Total Environment*, *571*, 791–800. https://doi.org/10.1016/j.scitotenv.2016.07.053

Dupas, R., Tittel, J., Jordan, P., Musolff, A., & Rode, M. (2018). Non-domestic phosphorus release in rivers during low-flow: Mechanisms and implications for sources identification. *Journal of Hydrology*, *560*, 141–149. https://doi.org/10.1016/j.jhydrol.2018.03.023

Ebeling, P. (2021a). *CCDB—catchment characteristics data base Germany*. HydroShare. https://doi.org/10.4211/hs.0fc1b5b1be4a475aacfd9545e72e6839

Ebeling, P. (2021b). *WQQDB—water quality metrics for catchments across Germany*. HydroShare. https://doi.org/10.4211/hs.9b4deeca259b4f7398ce72121b4e2979

EEA. (2013). DEM over Europe from the GMES RDA project (EU-DEM, resolution 25m)—version 1, Oct. 2013.

EEA. (2016a). CORINE land cover 2012 v18.5. Retrieved from https://land.copernicus.eu/pan-european/corine-land-cover

EEA. (2016b). EU-Hydro river network [geodata]. Retrieved from https://land.copernicus.eu/imagery-in-situ/eu-hydro/eu-hydro-public-beta/eu-hydro-river-network

EEA. (2018). European waters. Assessment of status and pressures 2018 (EEA Report No 7/201). European Environment Agency. Retrieved from https://www.eea.europa.eu/publications/state-of-water

EEA. (2019). The European environment—state and outlook 2020 (ISBN: 978-92-9480-090-9). European Environment Agency. Retrieved from https://www.eea.europa.eu/publications/soer-2020

EEC. (1991a). Council Directive 91/271/EEC of 21 May 1991 concerning urban waste water treatment. European Economic Community.

EEC. (1991b). Council Directive 91/676/EEC of 12 December 1991 concerning the protection of waters against pollution caused by nitrates from agricultural sources. European Economic Community.

EEC. (2000). Directive 2000/60/EC of the European parliament and of the council of 23 October 2000 establishing a framework for community action in the field of water policy. *Official Journal of the European Communities - Legislation*, *327*, 1–73.

Ehrhardt, S., Kumar, R., Fleckenstein, J. H., Attinger, S., & Musolff, A. (2019). Trajectories of nitrate input and output in three nested catchments along a land use gradient. *Hydrology and Earth System Sciences*, *23*(9), 3503–3524. https://doi.org/10.5194/hess-23-3503-2019

EPA. (2017). National water quality inventory: Report to congress. Retrieved from https://www.epa.gov/sites/production/files/2017-12/documents/305brtc_finalowow_08302017.pdf

Evans, D. M., Schoenholtz, S. H., Wigington, P. J., Griffith, S. M., & Floyd, W. C. (2014). Spatial and temporal patterns of dissolved nitrogen and phosphorus in surface waters of a multi-land use basin. *Environmental Monitoring and Assessment*, *186*(2), 873–887. https://doi.org/10.1007/s10661-013-3428-4

FAO/IIASA/ISRIC/ISSCAS/JRC. (2012). Harmonized world soil Database (version 1.2). Retrieved from https://webarchive.iiasa.ac.at/Research/LUC/External-World-soil-database/HTML/

Fischer, P., Pöthig, R., & Venohr, M. (2017). The degree of phosphorus saturation of agricultural soils in Germany: Current and future risk of diffuse P loss and implications for soil P management in Europe. *The Science of the Total Environment*, *599–600*, 1130–1139. https://doi.org/10.1016/j.scitotenv.2017.03.143

Galloway, J. N., Aber, J. D., Erisman, J. W., Seitzinger, S. P., Howarth, R. W., Cowling, E. B., & Cosby, B. J. (2003). The nitrogen cascade. *BioScience*, *53*(4), 341–356. https://doi.org/10.1641/0006-3568(2003)053[0341:tnc]2.0.co;2

Gentry, L. E., David, M. B., Royer, T. V., Mitchell, C. A., & Starks, K. M. (2007). Phosphorus transport pathways to streams in tile-drained agricultural watersheds. *Journal of Environmental Quality*, *36*(2), 408–415. https://doi.org/10.2134/jeq2006.0098

Godsey, S. E., Hartmann, J., & Kirchner, J. W. (2019). Catchment chemostasis revisited: Water quality responds differently to variations in weather and climate. *Hydrological Processes*, *33*(24), 3056–3069. https://doi.org/10.1002/hyp.13554

Godsey, S. E., Kirchner, J. W., & Clow, D. W. (2009). Concentration-discharge relationships reflect chemostatic characteristics of US catchments. *Hydrological Processes*, *23*(13), 1844–1864. https://doi.org/10.1002/hyp.7315

Gomez-Velez, J. D., Harvey, J. W., Cardenas, M. B., & Kiel, B. (2015). Denitrification in the Mississippi river network controlled by flow through river bedforms. *Nature Geoscience*, *8*, 941. https://doi.org/10.1038/ngeo2567

Greenwell, B. M. (2017). pdp: An R package for constructing partial dependence plots. *The R Journal*, *9*(1), 421–436. https://doi.org/10.32614/rj-2017-016

Gruber, N., & Galloway, J. N. (2008). An earth-system perspective of the global nitrogen cycle. *Nature*, *451*, 293. https://doi.org/10.1038/nature06592

Gu, S., Gruau, G., Dupas, R., Rumpel, C., Crème, A., Fovet, O., et al. (2017). Release of dissolved phosphorus from riparian wetlands: Evidence for complex interactions among hydroclimate variability, topography and soil properties. *The Science of the Total Environment*, *598*, 421–431. https://doi.org/10.1016/j.scitotenv.2017.04.028

Gücker, B., Brauns, M., & Pusch, M. T. (2006). Effects of wastewater treatment plant discharge on ecosystem structure and function of lowland streams. *Journal of the North American Benthological Society*, *25*(2), 313–329. https://doi.org/10.1899/0887-3593(2006)25[313:eowtpd]2.0.co;2

Gupta, H. V., Perrin, C., Blöschl, G., Montanari, A., Kumar, R., Clark, M., & Andréassian, V. (2014). Large-sample hydrology: A need to balance depth with breadth. *Hydrology and Earth System Sciences*, *18*(2), 463–477. https://doi.org/10.5194/hess-18-463-2014

Hannappel, S., Köpp, C., & Bach, T. (2018). Charakterisierung des Nitratabbauvermögens der Grundwasserleiter in Sachsen-Anhalt. *Grundwasser*, *23*(4), 311–321. https://doi.org/10.1007/s00767-018-0402-7

Hansen, A. T., Dolph, C. L., Foufoula-Georgiou, E., & Finlay, J. C. (2018). Contribution of wetlands to nitrate removal at the watershed scale. *Nature Geoscience*, *11*(2), 127–132. https://doi.org/10.1038/s41561-017-0056-6

Häußermann, U., Bach, M., Klement, L., & Breuer, L. (2019). *Stickstoff-Flächenbilanzen für Deutschland mit Regionalgliederung Bundesländer und Kreise—Jahre 1995 bis 2017*. Methodik, Ergebnisse und Minderungsmaßnahmen. Texte, 131/2019. Retrieved from https://www.umweltbundesamt.de/sites/default/files/medien/1410/publikationen/2019-10-28_texte_131-2019_stickstoffflaechenbilanz.pdf

Herndon, E. M., Dere, A. L., Sullivan, P. L., Norris, D., Reynolds, B., & Brantley, S. L. (2015). Landscape heterogeneity drives contrasting concentration-discharge relationships in shale headwater catchments. *Hydrology and Earth System Sciences*, *19*(8), 3333–3347. https://doi.org/10.5194/hess-19-3333-2015

Howden, N. J. K., Burt, T. P., Worrall, F., Whelan, M. J., & Bieroza, M. (2010). Nitrate concentrations and fluxes in the river Thames over 140 years (1868–2008): Are increases irreversible? *Hydrological Processes*, *24*(18), 2657–2662. https://doi.org/10.1002/hyp.7835

Hunsaker, C. T., & Johnson, D. W. (2017). Concentration-discharge relationships in headwater streams of the Sierra Nevada, California. *Water Resources Research*, *53*(9), 7869–7884. https://doi.org/10.1002/2016wr019693

Jarvie, H. P., Sharpley, A. N., Scott, J. T., Haggard, B. E., Bowes, M. J., & Massey, L. B. (2012). Within-river phosphorus retention: Accounting for a missing piece in the watershed phosphorus puzzle. *Environmental Science and Technology*, *46*(24), 13284–13292. https://doi.org/10.1021/es303562y

Jarvie, H. P., Sharpley, A. N., Withers, P. J. A., Scott, J. T., Haggard, B. E., & Neal, C. (2013). Phosphorus mitigation to control river eutrophication: Murky waters, inconvenient truths, and "postnormal" science. *Journal of Environmental Quality*, *42*(2), 295–304. https://doi.org/10.2134/jeq2012.0085

Jenny, J.-P., Anneville, O., Arnaud, F., Baulaz, Y., Bouffard, D., Domaizon, I., et al. (2020). Scientists' warning to humanity: Rapid degradation of the world's large lakes. *Journal of Great Lakes Research*, *46*(4), 686–702. https://doi.org/10.1016/j.jglr.2020.05.006

Jordan, P., Menary, W., Daly, K., Kiely, G., Morgan, G., Byrne, P., & Moles, R. (2005). Patterns and processes of phosphorus transfer from Irish grassland soils to rivers-integration of laboratory and catchment studies. *Journal of Hydrology*, *304*(1), 20–34. https://doi.org/10.1016/j.jhydrol.2004.07.021

Kirchner, J. W., Feng, X., Neal, C., & Robson, A. J. (2004). The fine structure of water-quality dynamics: The(high-frequency) wave of the future. *Hydrological Processes*, *18*(7), 1353–1359. https://doi.org/10.1002/hyp.5537

Knoll, L., Breuer, L., & Bach, M. (2019). Large scale prediction of groundwater nitrate concentrations from spatial data using machine learning. *The Science of the Total Environment*, *668*, 1317–1327. https://doi.org/10.1016/j.scitotenv.2019.03.045

Knoll, L., Breuer, L., & Bach, M. (2020). Nation-wide estimation of groundwater redox conditions and nitrate concentrations through machine learning. *Environmental Research Letters*, *15*(6), 064004. https://doi.org/10.1088/1748-9326/ab7d5c

Kuhn, M., Wing, J., Weston, S., Williams, A., Keefer, C., Engelhardt, A., et al. (2019). *caret: Classification and regression training*. Astrophysics Source Code Library. Retrieved from https://CRAN.R-project.org/package=caret

Kunkel, R., Bach, M., Behrendt, H., & Wendland, F. (2004). Groundwater-borne nitrate intakes into surface waters in Germany. *Water Science and Technology*, *49*(3), 11–19. https://doi.org/10.2166/wst.2004.0152

Laudon, H., Berggren, M., Ågren, A., Buffam, I., Bishop, K., Grabs, T., et al. (2011). Patterns and dynamics of dissolved organic carbon (DOC) in boreal streams: The role of processes, connectivity, and scaling. *Ecosystems*, *14*(6), 880–893. https://doi.org/10.1007/s10021-011-9452-8

Laudon, H., Köhler, S., & Buffam, I. (2004). Seasonal TOC export from seven boreal catchments in northern Sweden. *Aquatic Sciences: Research Across Boundaries*, *66*(2), 223–230. https://doi.org/10.1007/s00027-004-0700-2

Le Moal, M., Gascuel-Odoux, C., Ménesguen, A., Souchon, Y., Étrillard, C., Levain, A., et al. (2019). Eutrophication: A new wine in an old bottle? *The Science of the Total Environment*, *651*, 1–11. https://doi.org/10.1016/j.scitotenv.2018.09.139

Livneh, B., Kumar, R., & Samaniego, L. (2015). Influence of soil textural properties on hydrologic fluxes in the Mississippi river basin. *Hydrological Processes*, *29*(21), 4638–4655. https://doi.org/10.1002/hyp.10601

Marinos, R. E., Van Meter, K. J., & Basu, N. B. (2020). Is the river a chemostat?: Scale versus land use controls on nitrate concentration-discharge dynamics in the upper Mississippi river basin. *Geophysical Research Letters*, *47*(16), e2020GL087051. https://doi.org/10.1029/2020gl087051

McClain, M. E., Boyer, E. W., Dent, C. L., Gergel, S. E., Grimm, N. B., Groffman, P. M., et al. (2003). Biogeochemical hot spots and hot moments at the interface of terrestrial and aquatic ecosystems. *Ecosystems*, *6*(4), 301–312. https://doi.org/10.1007/s10021-003-0161-9

Meals, D. W., Dressing, S. A., & Davenport, T. E. (2010). Lag time in water quality response to best management practices: A review. *Journal of Environmental Quality*, *39*(1), 85–96. https://doi.org/10.2134/jeq2009.0108

Merz, C., Steidl, J., & Dannowski, R. (2009). Parameterization and regionalization of redox based denitrification for GIS-embedded nitrate transport modeling in Pleistocene aquifer systems. *Environmental Geology*, *58*(7), 1587. https://doi.org/10.1007/s00254-008-1665-6

Minaudo, C., Dupas, R., Gascuel-Odoux, C., Roubeix, V., Danis, P.-A., & Moatar, F. (2019). Seasonal and event-based concentration-discharge relationships to identify catchment controls on nutrient export regimes. *Advances in Water Resources*, *131*, 103379. https://doi.org/10.1016/j.advwatres.2019.103379

Moatar, F., Abbott, B. W., Minaudo, C., Curie, F., & Pinay, G. (2017). Elemental properties, hydrology, and biology interact to shape concentration-discharge curves for carbon, nutrients, sediment, and major ions. *Water Resources Research*, *53*(2), 1270–1287. https://doi.org/10.1002/2016wr019635

Moatar, F., Floury, M., Gold, A. J., Meybeck, M., Renard, B., Ferréol, M., et al. (2020). Stream solutes and particulates export regimes: A new framework to optimize their monitoring. *Frontiers in Ecology and Evolution*, *7*(516). https://doi.org/10.3389/fevo.2019.00516

Møller, A. B., Beucher, A., Iversen, B. V., & Greve, M. H. (2018). Predicting artificially drained areas by means of a selective model ensemble. *Geoderma*, *320*, 30–42.

Musolff, A. (2020). *WQQDB - water quality and quantity data base Germany: Metadata*. HydroShare. https://doi.org/10.4211/hs.a42addcbd59a466a9aa56472dfef8721

Musolff, A., Fleckenstein, J. H., Opitz, M., Büttner, O., Kumar, R., & Tittel, J. (2018). Spatio-temporal controls of dissolved organic carbon stream water concentrations. *Journal of Hydrology*, *566*, 205–215. https://doi.org/10.1016/j.jhydrol.2018.09.011

Musolff, A., Fleckenstein, J. H., Rao, P. S. C., & Jawitz, J. W. (2017). Emergent archetype patterns of coupled hydrologic and biogeochemical responses in catchments. *Geophysical Research Letters*, *44*(9), 4143–4151. https://doi.org/10.1002/2017gl072630

Musolff, A., Grau, T., Weber, M., Ebeling, P., Samaniego-Eguiguren, L., & Kumar, R. (2020). *WQQDB: Water quality and quantity data base Germany*. HydroShare. Retrieved from http://www.ufz.de/record/dmp/archive/7754

Musolff, A., Schmidt, C., Selle, B., & Fleckenstein, J. H. (2015). Catchment controls on solute export. *Advances in Water Resources*, *86*, 133–146. https://doi.org/10.1016/j.advwatres.2015.09.026

Oelsner, G. P., Sprague, L. A., Murphy, J. C., Zuellig, R. E., Johnson, H. M., Ryberg, K. R., et al. (2017). *Water-quality trends in the nation's rivers and streams, 1972–2012—data preparation, statistical methods, and trend results*. U.S. Geological Survey Scientific Investigations. Retrieved from https://doi.org/10.3133/sir20175006

Oldham, C. E., Farrow, D. E., & Peiffer, S. (2013). A generalized Damköhler number for classifying material processing in hydrological systems. *Hydrology and Earth System Sciences*, *17*(3), 1133–1148. https://doi.org/10.5194/hess-17-1133-2013

Onderka, M., Wrede, S., Rodný, M., Pfister, L., Hoffmann, L., & Krein, A. (2012). Hydrogeologic and landscape controls of dissolved inorganic nitrogen (DIN) and dissolved silica (DSi) fluxes in heterogeneous catchments. *Journal of Hydrology*, *450–451*, 36–47. https://doi.org/10.1016/j.jhydrol.2012.05.035

Osterholz, W. R., Hanrahan, B. R., & King, K. W. (2020). Legacy phosphorus concentration-discharge relationships in surface runoff and tile drainage from Ohio crop fields. *Journal of Environmental Quality*, *49*(3), 675–687. https://doi.org/10.1002/jeq2.20070

Ouedraogo, I., Defourny, P., & Vanclooster, M. (2019). Application of random forest regression and comparison of its performance to multiple linear regression in modeling groundwater nitrate concentration at the African continent scale. *Hydrogeology Journal*, *27*(3), 1081–1098. https://doi.org/10.1007/s10040-018-1900-5

Pflugmacher, D., Rabe, A., Peters, M., & Hostert, P. (2018). *Pan-European land cover map of 2015 based on Landsat and LUCAS data*. PANGAEA. Retrieved from https://doi.org/10.1594/PANGAEA.896282

Pinay, G., Peiffer, S., De Dreuzy, J.-R., Krause, S., Hannah, D. M., Fleckenstein, J. H., et al. (2015). Upscaling nitrogen removal capacity from local hotspots to low stream orders' drainage basins. *Ecosystems*, *18*(6), 1101–1120. https://doi.org/10.1007/s10021-015-9878-5

Rivett, M. O., Buss, S. R., Morgan, P., Smith, J. W. N., & Bemment, C. D. (2008). Nitrate attenuation in groundwater: A review of biogeochemical controlling processes. *Water Research*, *42*(16), 4215–4232. https://doi.org/10.1016/j.watres.2008.07.020

Rodriguez-Galiano, V., Mendes, M. P., Garcia-Soldado, M. J., Chica-Olmo, M., & Ribeiro, L. (2014). Predictive modeling of groundwater nitrate pollution using random forest and multisource variables related to intrinsic and specific vulnerability: A case study in an agricultural setting (Southern Spain). *The Science of the Total Environment*, *476–477*, 189–206. https://doi.org/10.1016/j.scitotenv.2014.01.001

Rose, L. A., Karwan, D. L., & Godsey, S. E. (2018). Concentration-discharge relationships describe solute and sediment mobilization, reaction, and transport at event and longer timescales. *Hydrological Processes*, *32*(18), 2829–2844. https://doi.org/10.1002/hyp.13235

Sabater, S., Butturini, A., Clement, J.-C., Burt, T., Dowrick, D., Hefting, M., et al. (2003). Nitrogen removal by Riparian buffers along a European climatic gradient: Patterns and factors of variation. *Ecosystems*, *6*(1), 0020–0030. https://doi.org/10.1007/s10021-002-0183-8

Samaniego, L., Kumar, R., & Attinger, S. (2010). Multiscale parameter regionalization of a grid-based hydrologic model at the mesoscale. *Water Resources Research*, *46*(5). https://doi.org/10.1029/2008wr007327

Schmidt, L., Heße, F., Attinger, S., & Kumar, R. (2020). Challenges in applying machine learning models for hydrological inference: A case study for flooding events across Germany. *Water Resources Research*, *56*, e2019WR025924. https://doi.org/10.1029/2019WR025924

Schoumans, O. F., Bouraoui, F., Kabbe, C., Oenema, O., & van Dijk, K. C. (2015). Phosphorus management in Europe in a changing world. *Ambio*, *44*(2), 180–192. https://doi.org/10.1007/s13280-014-0613-9

Schoumans, O. F., Chardon, W. J., Bechmann, M. E., Gascuel-Odoux, C., Hofman, G., Kronvang, B., et al. (2014). Mitigation options to reduce phosphorus losses from the agricultural sector and improve surface water quality: A review. *The Science of the Total Environment*, *468–469*, 1255–1266. https://doi.org/10.1016/j.scitotenv.2013.08.061

Seibert, J., Grabs, T., Köhler, S., Laudon, H., Winterdahl, M., & Bishop, K. (2009). Linking soil- and stream-water chemistry based on a riparian flow-concentration integration model. *Hydrology and Earth System Sciences*, *13*(12), 2287–2297. https://doi.org/10.5194/hess-13-2287-2009

Shangguan, W., Hengl, T., Mendes de Jesus, J., Yuan, H., & Dai, Y. (2017). Mapping the global depth to bedrock for land surface modeling. *Journal of Advances in Modeling Earth Systems*, *9*(1), 65–88. https://doi.org/10.1002/2016ms000686

Sharpley, A., Jarvie, H. P., Buda, A., May, L., Spears, B., & Kleinman, P. (2013). Phosphorus legacy: Overcoming the effects of past management practices to mitigate future water quality impairment. *Journal of Environmental Quality*, *42*(5), 1308–1326. https://doi.org/10.2134/jeq2013.03.0098

Sivapalan, M. (2006). Pattern, process and function: Elements of a unified theory of hydrology at the catchment scale. In M. G. Anderson, & J. J. McDonnell (Eds.), *Encyclopedia of hydrological sciences*. John Wiley & Sons.

Smolders, E., Baetens, E., Verbeeck, M., Nawara, S., Diels, J., Verdievel, M., et al. (2017). Internal loading and redox cycling of sediment iron explain reactive phosphorus concentrations in lowland rivers. *Environmental Science and Technology*, *51*(5), 2584–2592. https://doi.org/10.1021/acs.est.6b04337

Solomon, C. T., Jones, S. E., Weidel, B. C., Buffam, I., Fork, M. L., Karlsson, J., et al. (2015). Ecosystem consequences of changing inputs of terrestrial dissolved organic matter to lakes: Current knowledge and future challenges. *Ecosystems*, *18*(3), 376–389. https://doi.org/10.1007/s10021-015-9848-y

Stanley, E. H., Powers, S. M., Lottig, N. R., Buffam, I., & Crawford, J. T. (2012). Contemporary changes in dissolved organic carbon (DOC) in human-dominated rivers: is there a role for DOC management?. *Freshwater Biology*, *57*(s1), 26–42. https://doi.org/10.1111/j.1365-2427.2011.02613.x

Taylor, P. G., & Townsend, A. R. (2010). Stoichiometric control of organic carbon-nitrate relationships from soils to the sea. *Nature*, *464*, 1178. https://doi.org/10.1038/nature08985

Team, R. C. (2019). *R: A language and environment for statistical computing*. R Foundation for Statistical Computing. Retrieved from https://www.R-project.org/

Thompson, S. E., Basu, N. B., Lascurain, J., Aubeneau, A., & Rao, P. S. C. (2011). Relative dominance of hydrologic versus biogeochemical factors on solute export across impact gradients. *Water Resources Research*, *47*(10). https://doi.org/10.1029/2010wr009605

Tunaley, C., Tetzlaff, D., & Soulsby, C. (2017). Scaling effects of riparian peatlands on stable isotopes in runoff and DOC mobilisation. *Journal of Hydrology*, *549*, 220–235. https://doi.org/10.1016/j.jhydrol.2017.03.056

Underwood, K. L., Rizzo, D. M., Schroth, A. W., & Dewoolkar, M. M. (2017). Evaluating spatial variability in sediment and phosphorus concentration-discharge relationships using Bayesian inference and self-organizing maps. *Water Resources Research*, *53*(12), 10293–10316. https://doi.org/10.1002/2017wr021353

Van der Velde, Y., Rooij, G. H. d., Rozemeijer, J. C., Geer, F. C. v., & Broers, H. P. (2010). Nitrate response of a lowland catchment: On the relation between stream concentration and travel time distribution dynamics. *Water Resources Research*, *46*(11). https://doi.org/10.1029/2010wr009105

Van Meter, K. J., & Basu, N. B. (2015). Catchment legacies and time lags: A parsimonious watershed model to predict the effects of legacy storage on nitrogen export. *PLoS One*, *10*(5), e0125971. https://doi.org/10.1371/journal.pone.0125971

Van Meter, K. J., & Basu, N. B. (2017). Time lags in watershed-scale nutrient transport: An exploration of dominant controls. *Environmental Research Letters*, *12*(8), 084017. https://doi.org/10.1088/1748-9326/aa7bf4. http://dx.doi.org/10.1088/1748-9326/aa7bf4

Vitousek, P. M., Mooney, H. A., Lubchenco, J., & Melillo, J. M. (1997). Human domination of earth's ecosystems. *Science*, *277*(5325), 494–499. https://doi.org/10.1126/science.277.5325.494

Vogel, R. M., Rudolph, B. E., & Hooper, R. P. (2005). Probabilistic behavior of water-quality loads. *Journal of Environmental Engineering*, *131*(7), 1081–1089. https://doi.org/10.1061/(asce)0733-9372(2005)131:7(1081)

Wallin, M. B., Weyhenmeyer, G. A., Bastviken, D., Chmiel, H. E., Peter, S., Sobek, S., & Klemedtsson, L. (2015). Temporal control on concentration, character, and export of dissolved organic carbon in two hemiboreal headwater streams draining contrasting catchments. *Journal of Geophysical Research: Biogeosciences*, *120*(5), 832–846. https://doi.org/10.1002/2014jg002814

Wen, H., Perdrial, J., Abbott, B. W., Bernal, S., Dupas, R., Godsey, S. E., et al. (2020). Temperature controls production but hydrology regulates export of dissolved organic carbon at the catchment scale. *Hydrology and Earth System Sciences*, *24*(2), 945–966. https://doi.org/10.5194/hess-24-945-2020

Wendland, F., Blum, A., Coetsiers, M., Gorova, R., Griffioen, J., Grima, J., et al. (2008). European aquifer typology: A practical framework for an overview of major groundwater composition at European scale. *Environmental Geology*, *55*(1), 77–85. https://doi.org/10.1007/s00254-007-0966-5

Westphal, K., Graeber, D., Musolff, A., Fang, Y., Jawitz, J. W., & Borchardt, D. (2019). Multi-decadal trajectories of phosphorus loading, export, and instream retention along a catchment gradient. *The Science of the Total Environment*, *667*, 769–779. https://doi.org/10.1016/j.scitotenv.2019.02.428

Wilde, S., Hansen, C., & Bergmann, A. (2017). Nachlassender Nitratabbau im Grundwasser und deren Folgen—abgestufte modellgestützte Bewertungsansätze. *Grundwasser*, *22*(4), 293–308. https://doi.org/10.1007/s00767-017-0373-0

Winterdahl, M., Erlandsson, M., Futter, M. N., Weyhenmeyer, G. A., & Bishop, K. (2014). Intra-annual variability of organic carbon concentrations in running waters: Drivers along a climatic gradient. *Global Biogeochemical Cycles*, *28*(4), 451–464. https://doi.org/10.1002/2013gb004770

Winterdahl, M., Futter, M., Köhler, S., Laudon, H., Seibert, J., & Bishop, K. (2011). Riparian soil temperature modification of the relationship between flow and dissolved organic carbon concentration in a boreal stream. *Water Resources Research*, *47*(8). https://doi.org/10.1029/2010wr010235

Withers, P. J. A., & Jarvie, H. P. (2008). Delivery and cycling of phosphorus in rivers: A review. *The Science of the Total Environment*, *400*(1), 379–395. https://doi.org/10.1016/j.scitotenv.2008.08.002

WMO. (2008). *Manual on low-flow estimation and prediction*. World Meteorological Organization. Retrieved from http://library.wmo.int/pmb_ged/wmo_1029_en.pdf

Wold, S., Sjöström, M., & Eriksson, L. (2001). PLS-regression: A basic tool of chemometrics. *Chemometrics and Intelligent Laboratory Systems*, *58*(2), 109–130. https://doi.org/10.1016/s0169-7439(01)00155-1

Zarnetske, J. P., Bouda, M., Abbott, B. W., Saiers, J., & Raymond, P. A. (2018). Generality of hydrologic transport limitation of watershed organic carbon flux across ecoregions of the United States. *Geophysical Research Letters*, *45*(21), 11702–11711. https://doi.org/10.1029/2018gl080005

Zhi, W., Li, L., Dong, W., Brown, W., Kaye, J., Steefel, C., & Williams, K. H. (2019). Distinct source water chemistry shapes contrasting concentration-discharge patterns. *Water Resources Research*, *55*(5), 4233–4251. https://doi.org/10.1029/2018wr024257

Zimmer, M. A., Pellerin, B., Burns, D. A., & Petrochenkov, G. (2019). Temporal variability in nitrate-discharge relationships in large rivers as revealed by high-frequency data. *Water Resources Research*. *55*, 973–989. https://doi.org/10.1029/2018WR023478

Zink, M., Kumar, R., Cuntz, M., & Samaniego, L. (2017). A high-resolution dataset of water fluxes and states for Germany accounting for parametric uncertainty. *Hydrology and Earth System Sciences*, *21*(3), 1769–1790. https://doi.org/10.5194/hess-21-1769-2017